THE JOURNAL OF BIOLOGICAL CHEMISTRY VOL. 287, NO. 7, pp. 5079–5090, February 10, 2012

Three-dimensional Structure of Nylon Hydrolase and Mechanism of Nylon-6 Hydrolysis*[S]

Received for publication, November 8, 2011, and in revised form, December 16, 2011 Published, JBC Papers in Press, December 19, 2011, DOI 10.1074/jbc.M111.321992

Seiji Negoro[‡1,2], Naoki Shibata[§¶1], Yusuke Tanaka[‡1], Kengo Yasuhira[‡1], Hiroshi Shibata[‡], Haruka Hashimoto[‡], Young-Ho Lee[‖], Shohei Oshima[**], Ryuji Santa[‡], Shohei Oshima[‡], Kozo Mochiji[**], Yuji Goto[‖], Takahisa Ikegami[‖], Keisuke Nagai[‡], Dai-ichiro Kato[‡], Masahiro Takeo[‡], and Yoshiki Higuchi[§¶3]

From the [‡]Department of Materials Science and Chemistry, Graduate School of Engineering, University of Hyogo, Hyogo 671-2280, the [§]Department of Life Science, Graduate School of Life Science, University of Hyogo, Hyogo 678-1297, the [¶]RIKEN Harima Institute, SPring-8 Center, Hyogo 679-5148, the [‖]Institute for Protein Research, Osaka University, Osaka 565-0871, and the [**]Department of Intelligence Mechanical Technology, Graduate School of Engineering, University of Hyogo, Hyogo 671-2280, Japan

Background: Biodegradation of polyamides is important from the industrial and environmental point of view.
Results: We identified the catalytic residue of nylon hydrolase as Thr-267 and enhanced the protein thermostability by 36 °C (T_m = 88 °C) by introducing mutations at the subunit interfaces of tetramer structure.
Conclusion: We revealed the mechanism of nylon-6 hydrolysis.
Significance: We established an approach to biodegrade polymeric nylon-6.

We performed x-ray crystallographic analyses of the 6-aminohexanoate oligomer hydrolase (NylC) from *Agromyces* sp. at 2.0 Å-resolution. This enzyme is a member of the N-terminal nucleophile hydrolase superfamily that is responsible for the degradation of the nylon-6 industry byproduct. We observed four identical heterodimers (27 kDa + 9 kDa), which resulted from the autoprocessing of the precursor protein (36 kDa) and which constitute the doughnut-shaped quaternary structure. The catalytic residue of NylC was identified as the N-terminal Thr-267 of the 9-kDa subunit. Furthermore, each heterodimer is folded into a single domain, generating a stacked $\alpha\beta\beta\alpha$ core structure. Amino acid mutations at subunit interfaces of the tetramer were observed to drastically alter the thermostability of the protein. In particular, four mutations (D122G/H130Y/D36A/E263Q) of wild-type NylC from *Arthrobacter* sp. (plasmid pOAD2-encoding enzyme), with a heat denaturation temperature of T_m = 52 °C, enhanced the protein thermostability by 36 °C (T_m = 88 °C), whereas a single mutation (G111S or L137A) decreased the stability by ~10 °C. We examined the enzymatic hydrolysis of nylon-6 by the thermostable NylC mutant. Argon cluster secondary ion mass spectrometry analyses of the reaction products revealed that the major peak of nylon-6 (m/z 10,000–25,000) shifted to a smaller range, producing a new peak corresponding to m/z 1500–3000 after the enzyme treatment at 60 °C. In addition, smaller fragments in the soluble fraction were successively hydrolyzed to dimers and monomers. Based on these data, we propose that NylC should be designated as nylon hydrolase (or nylonase). Three potential uses of NylC for industrial and environmental applications are also discussed.

Nylons are synthetic polymers that contain recurring amide groups (R-CO-NH-R′) as integral parts of their main polymer chains. The high strength, elasticity, abrasion resistance, chemical resistance, and shape-holding characteristics of nylons over wide temperature ranges make these polymers suitable for the production of fibers and plastics. Currently, the worldwide production of nylons is estimated to be three to four million tons per year. Nylons tend to be partially crystalline, and the degree of crystallinity affects the properties of nylons, such as the melting points, strength, and rigidity. Two forms of crystals (α and γ) have been reported (1). In the α-form, each polymer chain is stabilized by hydrogen bonds with adjacent chains aligned in an antiparallel orientation, whereas the chains are parallel in the γ-form. The α-form of nylon-6 is generally more stable (1).

Nylon-6 is produced by the ring cleavage polymerization of ϵ-caprolactam and consists of more than 100 units of 6-aminohexanoate (Ahx).[4] However, during the polymerization reac-

* This work was supported in part by a grant-in-aid for scientific research (Japan Society for Promotion of Science) and grants from the Global Center of Excellence Program and the Japan Aerospace Exploration Agency project.

[S] This article contains supplemental Tables S1–S4 and Figs. S1–S5.

The atomic coordinates and structure factors (code 3AXG) have been deposited in the Protein Data Bank, Research Collaboratory for Structural Bioinformatics, Rutgers University, New Brunswick, NJ (http://www.rcsb.org/).

[1] These authors contributed equally to this work.
[2] To whom correspondence may be addressed: Dept. of Materials Science and Chemistry, Graduate School of Engineering, University of Hyogo, 2167 Shosha, Himeji, Hyogo 671-2280, Japan. Tel./Fax: 81-792-67-4891; E-mail: negoro@eng.u-hyogo.ac.jp.
[3] To whom correspondence may be addressed: Dept. of Life Science, Graduate School of Life Science, University of Hyogo, 3-2-1 Koto, Kamigori-cho, Ako-gun, Hyogo 678-1297, Japan. Tel./Fax: 81-791-58-0179; E-mail: hig@sci.u-hyogo.ac.jp.

[4] The abbreviations used are: Ahx, 6-aminohexanoate; N-tn, N-terminal nucleophile; NylA, 6-aminohexanoate cyclic dimer hydrolase; NylB, 6-aminohexanoate-linear dimer hydrolase; NylC, 6-aminohexanoate oligomer hydrolase, or nylon hydrolase; r.m.s., root mean square; DmpA, L-aminopeptidase D-Ala-esterase/amidase; BapA, β-peptidyl aminopeptidase; OAT, ornithine acetyltransferase; SIMS, secondary ion mass spectrometry; S^{111}, G111S; G^{122}, D122G; Y^{130}, H130Y; A^{137}, L137A; M^{225}, V225M; $G^{122}Y^{130}$, D122G/H130Y; $G^{122}Y^{130}A^{36}$, D122G/H130Y/D36A; $G^{122}Y^{130}Q^{263}$, D122G/H130Y/E263Q; $G^{122}Y^{130}M^{225}$, D122G/H130Y/V225M; $S^{111}G^{122}Y^{130}$, G111S/D122G/H130Y; $G^{122}Y^{130}A^{137}$, D122G/H130Y/L137A; $G^{122}Y^{130}A^{36}Q^{263}$, D122G/H130Y/D36A/E263Q; $S^{111}G^{122}Y^{130}A^{137}$, G111S/D122G/H130Y/L137A.

tion, some molecules fail to polymerize and remain oligomers, whereas others undergo head-to-tail condensation to form cyclic oligomers. We have isolated bacterial strains that can degrade Ahx oligomers, which are by-products of nylon-6 production, and use these oligomers as their sole carbon and nitrogen source (2–6). Previous biochemical studies have revealed that three enzymes, NylABC, are responsible for the degradation of the by-products produced during nylon-6 manufacturing. The Ahx cyclic dimer hydrolase (NylA; EC 3.5.2.12), a member of the amidase signature hydrolase family, specifically hydrolyzes one of the two equivalent amide bonds in the Ahx cyclic dimer, generating an Ahx linear dimer (7). The Ahx dimer hydrolase (NylB; EC 3.5.1.46), a member of the penicillin-recognizing family of serine reactive hydrolases, hydrolyzes Ahx oligomers by an exo-type mode (8–12). The Ahx oligomer hydrolase (NylC; EC 3.5.-.-) degrades Ahx cyclic and linear oligomers with a degree of polymerization greater than three by an endo-type mode (5, 13–15).

NylC has been found in *Arthrobacter* (pOAD2 plasmid-encoded NylC; $NylC_{p2}$), *Agromyces* ($NylC_A$), and *Kocuria* ($NylC_K$) (5). These enzymes are each encoded by a single gene that corresponds to a polypeptide chain of 355 amino acids. However, the post-translational cleavage of the nascent polypeptide between Asn-266 and Thr-267 generates a 27-kDa (α)-subunit and a 9-kDa (β)-subunit (5, 14). The autoprocessing of the inactive precursor to an active enzyme is a specific feature of the N-terminal nucleophile (N-tn) hydrolase family (16–33). $NylC_A$ and $NylC_K$ have 5 and 15 amino acid substitutions, respectively, relative to the $NylC_{p2}$ sequence (supplemental Fig. S1), and both have 10–20 °C higher thermostability than $NylC_{p2}$ (5).

Recently, we reported the crystallization conditions of $NylC_A$ that are suitable for x-ray crystallographic analyses (34). In this study, we performed x-ray crystallographic analyses of $NylC_A$, examined its structural/evolutional relationship to proteins registered in the Protein Data Bank (PDB), and estimated the residues responsible for the catalytic function and autoprocessing. We also analyzed the effect of amino acid mutations on the thermostability of NylC. Furthermore, we investigated the possibility of using the thermostable NylC mutant to degrade polymeric nylon-6 at high temperatures, which is expected to increase the reactivity of the polymer.

EXPERIMENTAL PROCEDURES

DNA Preparation and Site-directed Mutagenesis

The plasmids pSKFC4 ($NylC_{p2}$), pSKRC4 ($NylC_A$), and pSKKC4 ($NylC_K$) contained 1.1-kb genes flanked by BamHI and PstI restriction sites, which were cloned into the expression vector pBluescript II SK(+) (Stratagene, La Jolla, CA.) (5). *Escherichia coli* JM109-competent cells were prepared by the $CaCl_2$ method (35) and stored at −80 °C before use. To introduce the D36A, G111S, D122G, H130Y, L137A, V225M, and E263Q mutations into the $NylC_{p2}$ sequence, site-directed mutagenesis was performed using the PrimeSTAR mutagenesis kit (Takara Bio Inc.) with the primers listed in supplemental Table S1. The plasmids that contained the 1.1-kb fragments with mutated $NylC_{p2}$ were isolated from transformed *E. coli* JM109 cells. DNA sequencing confirmed that the desired mutations were introduced into the wild-type $nylC_{p2}$ sequence.

Cultivation, Enzyme Purification, and Enzyme Assay

Cultivation and purification from *E. coli* clones were performed as reported previously (34). In the NylC activity assays, the enzyme solution (0.1 ml) was mixed with an Ahx cyclic oligomer solution (0.9 ml, 4 mg ml^{-1} Ahx cyclic oligomer in 20 mM phosphate buffer, pH 7.3, 10% glycerol (buffer A)) and incubated at 30 °C (standard assay condition). An increase in the concentration of the amino group was determined using trinitrobenzene sulfonic acid (5). Kinetic studies were performed under standard assay conditions, with the exception of the different Ahx cyclic oligomer concentrations used.

Nylon Degradation Tests

Nylon-6 that was mechanically disintegrated to a powder was a generous gift from Toyobo Co. (Tsuruga, Japan). To analyze the particle sizes, the nylon sample was magnified 80-fold with a scanning electron microscope (Hitachi, model TM-1000). The diameter (maximum length) of 157 particles observed in five electron microphotographs was measured. The diameters ranged from 68 to 720 μm (average ± S.D., 270 ± 140 μm). To increase the reactivity of the nylon sample, the nylon-6 powder (10 mg) was autoclaved in plastic tubes (Eppendorf Co.) containing buffer A (180 μl) at 120 °C for 20 min prior to the initiation of the enzyme reaction. Hydrolytic reactions were initiated by the addition of the thermostable $NylC_{p2}$-$G^{122}Y^{130}A^{36}Q^{263}$ mutant enzyme (1 mg ml^{-1}, 20 μl) to each tube and incubated at 60 °C for 2 h. The gas cluster secondary ion mass spectrometry (SIMS) equipment (developed in the project "Development of System and Technology for Advanced Measurement and Analysis," Japan Science and Technology Agency, 2006–2010) was used to analyze the reaction products (36). Enzyme reactions were performed in triplicate. The reaction products (containing both the insoluble and the soluble fractions) from the first tube were spotted onto a silicon plate (1-cm^2 square plate). Mass-to-charge ratio (m/z) ranges of 5,000–35,000 and 0–1,500 were analyzed. The solid fractions (~10 mg) that were recovered from the reaction products (the second tube) were washed with distilled water, lyophilized, and dissolved in trifluoroethanol (0.2 ml). Subsequently, a fraction (0.02 ml) was spotted onto a silicon plate (1-cm^2 square plate). The m/z range of 1,500–15,000 was analyzed. The soluble fraction (1 μl) from the third tube was spotted onto a thin layer plate and developed by a solvent mixture containing 1-propanol:water:ethyl acetate:ammonia (24:12:4:1.3). The degradation products were detected by spraying the plate with a 0.2% ninhydrin solution (in *n*-butyl alcohol saturated with water) (5).

Crystallographic Analysis

Crystallization and Diffraction Data Collection—For analysis of $NylC_A$, plate-like crystals (0.8 × 0.4 × 0.3 mm) were obtained by the sitting-drop vapor diffusion method. Droplets were prepared by mixing 2 μl of purified $NylC_A$ solution (10 mg ml^{-1} protein in buffer A) and 2 μl of reservoir solution (1.0 M sodium citrate as a precipitant in 0.1 M HEPES buffer (pH 7.5), 0.2 M NaCl) and were equilibrated against 100 μl of reservoir

TABLE 1
Data collection statistics and refinement statistics
Values in parentheses are for the outer resolution shell.

		Native ($NylC_A$)	K_2PtCl_4 derivative ($NylC_A$)
Data collection statistics			
Space group		I222	I222
Unit cell (Å)			
a		155.86	155.99
b		214.45	214.72
c		478.80	477.82
Wavelength (Å)		1.0000	1.0000
Resolution (outer shell) (Å)		30-2.00 (2.07-2.00)	30-2.20 (2.28-2.20)
Total reflections		1,789,588	2,786,883
Unique reflections (outer shell)		501,977 (38,621)	398,011 (36,644)
Completeness (outer shell) (%)		94.3 (73.0)	99.0 (91.7)
R_{merge} (outer shell) (%)		11.1 (25.4)	6.4 (46.2)
$<I / \sigma(I)>$ (outer shell)		10.6 (2.32)	26.1 (2.87)
Multiplicity		3.6 (2.0)	7.0 (4.8)
Refinement statistics			
Resolution range (outer shell) (Å)	50-2.00 (2.07-2.00)		
R_{work}[a] (outer shell) (%)	22.3 (31.9)		
R_{free}[a] (outer shell) (%)	25.2 (33.5)		
No. of protein atoms	37,819		
No. of water molecules	3,006		
r.m.s. deviations from ideal values			
r.m.s. bond distances (Å)	0.006		
r.m.s. bond angles (°)	0.9		
Dihedral angles (°)	22.3		
Improper angles (°)	0.74		
Ramachandran plot			
Favored (%)	96.2		
Allowed (%)	99.9		
Outliers	4		

[a] $R = \Sigma_{hkl} \| |F_{obs}| - k|F_{calc}| \| (\Sigma_{hkl}|F_{obs}|)^{-1}$; k = scaling factor.

solution at 10 °C for 1 week. The crystal belonged to the space group I222, with unit cell parameters $a = 155.86$ Å, $b = 214.45$ Å, and $c = 478.80$ Å (Table 1).

For native crystals, the crystals were soaked for 24 h in a cryoprotectant solution (1.0 M sodium citrate, 0.1 M HEPES (pH 7.5), 0.2 M NaCl, 25% glycerol). Heavy atom derivatives of $NylC_A$ were prepared by soaking the crystals for 72 h in cryoprotectant solution containing 5 mM K_2PtCl_4. Cryo-cooling was performed by blowing cold nitrogen steam onto the crystals at 100 K.

The diffraction data sets were collected at the SPring-8 (Hyogo, Japan) beamline BL38B1 equipped with a Rigaku Jupiter CCD detector system. The following parameters were chosen for data collection: wavelength, 1.0000 Å; crystal to detector distance, 180 mm; oscillation range per image, 0.5° (for native and platinum derivative). Indexing, integration, and the scaling of reflections were performed using the HKL2000 program package (37). Diffraction data were collected from native $NylC_A$ crystals and from the K_2PtCl_4-derivative to resolutions of 2.00 Å and 2.20 Å, respectively (Table 1).

Phase Determination, Model Building, and Crystallographic Refinement—The NylC structure was determined by the single wavelength anomalous diffraction method using the K_2PtCl_4 derivative data. The platinum substructure for the derivative crystal was solved at a resolution of 2.2 Å by the program BnP (38) using the anomalous signal of the platinum atoms. Initial phase parameters were determined using the program SHARP (39). The electron density map was automatically traced with ARP/wARP. Models for the untraced regions, with the exception of the amino acids at positions 1–18 and 261–266, were constructed by manual model building using XFIT (40). Rigid body refinement was performed using the coordinates of the initial model to fit the unit cell of the $NylC_A$ crystal followed by positional and *B*-factor refinement with the program CNS (41). Non-crystallographic symmetry restraints were applied throughout refinement with the exception of the residues 25–40 and 131–137 in which significant structural differences among chains were detected.

After several cycles of manual model rebuilding by XFIT, *R*-factor and R_{free} were determined to be 18.1 and 19.5%. No residue was found in the outlying regions. The results of the crystal structure analysis are summarized in Table 1. The figures of the three-dimensional structural models were generated with the program MolFeat (version 3.6, FiatLux Co., Tokyo, Japan).

CD Analysis

Circular dichroism (CD) spectra at far-UV wavelengths (200–250 nm) were measured using a spectropolarimeter (JASCO, model J-720WI). A cuvette with a path length of 1 mm was used for far-UV CD measurements. The results are expressed as the mean residue molar ellipticity, $[\theta]$, which is defined as $[\theta] = 100\ (\theta_{obs} - \theta_{back})\ l^{-1}\ c^{-1}$, where θ_{obs} is the observed ellipticity in degrees, θ_{back} is the observed ellipticity in degrees in the absence of enzyme (as background), c is the molar concentration of the residue, and l is the length of the light path (in centimeters). The temperature was controlled at 25 °C with a JASCO PTC-348WI Peltier system. For thermal transition experiments, the temperature was shifted from 25 to 95 °C with a JASCO PTC-348WI Peltier system at 1 °C min^{-1}, and CD measurements were performed at 220 nm. The protein concentration used in the far-UV CD measurements was 0.1 mg ml^{-1}.

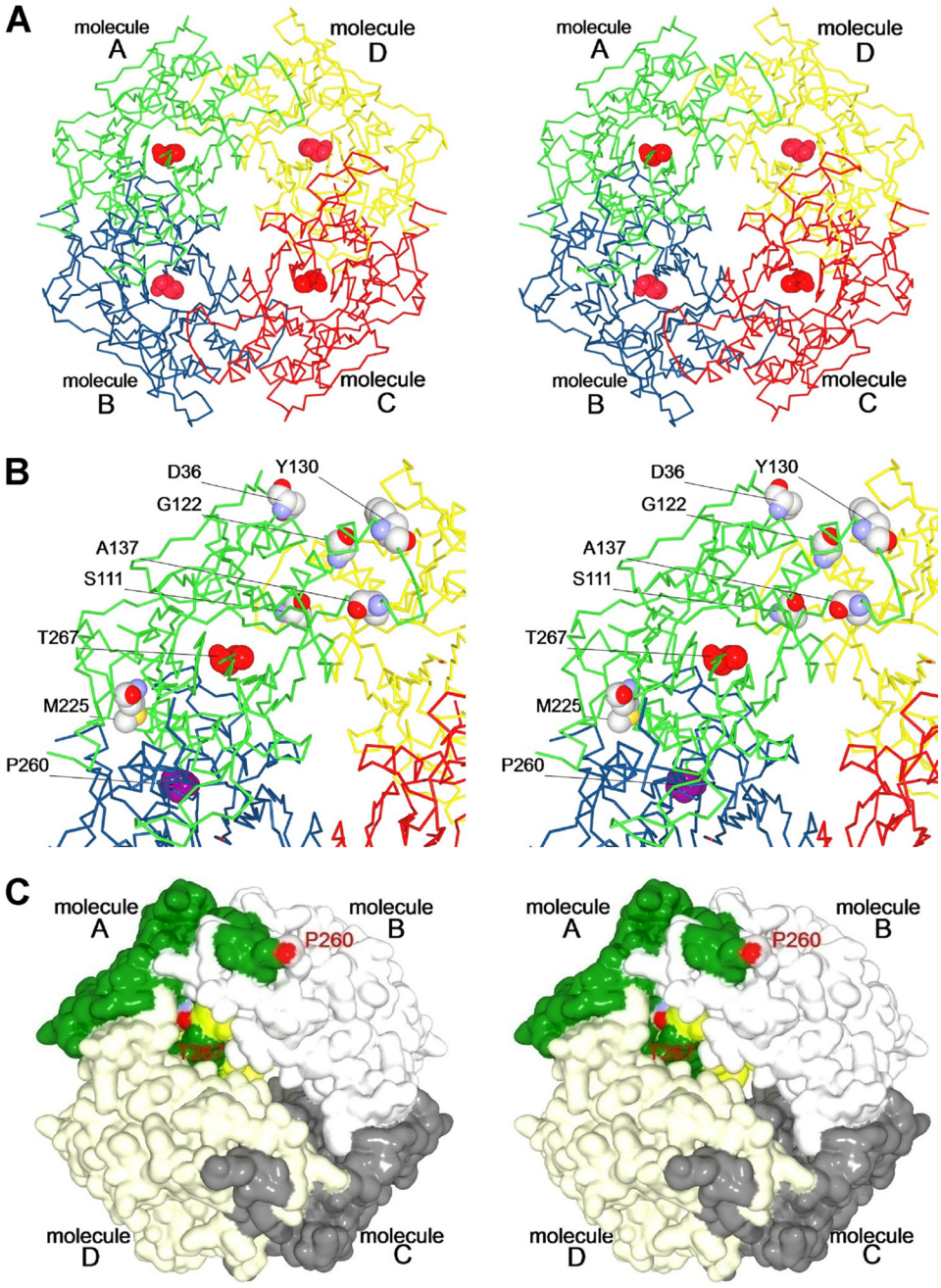

FIGURE 1. **Stereo view of quaternary structure of NylC$_A$.** *A*, the quaternary structure is shown, with different colors highlighting the individual molecules A (*green*), B (*blue*), C (*red*), and D (*yellow*). The catalytic residue Thr-267 (the N terminus of the β-subunit) is shown as a space-filling model (*red*). *B*, an enlarged view of molecule A and its interfaces with the adjacent molecules B and D. Six residues selected for mutagenesis (Asp-36 (Ala-36 in NylC$_K$), Ser-111, Gly-122, Tyr-130, Ala-137, and Met-225) are shown as space-filling models. Because of the poor electron density distribution of the C-terminal region in the α-subunit, including Glu-263 (Gln-263 in NylC$_K$), the adjacent Pro-260 is shown as a space-filling model (*magenta*). *C*, surface structure of NylC$_A$. The α-subunit and β-subunit in a single heterodimer (molecule A) are highlighted in *dark green* and *light green*, respectively. The other three heterodimers are shown in different shades of *gray*.

RESULTS AND DISCUSSION

Quaternary Structure

The asymmetric unit contains 15 molecules (molecules A–O), each composed of an α- and a β-subunit. One molecule (O) is part of a tetramer in which the four heterodimers are related by crystallographic 222 symmetry. Two molecules in dimer (M/N) form another tetramer that is related by a crystallographic two-fold axis, and the rest of the 12 molecules comprise three tetramers (A/B/C/D, E/F/G/H, and I/J/K/L) that are related by non-crystallographic 222 symmetries. The root mean square (r.m.s.) deviations of the superimposed C_α atoms for all 15 molecules were calculated to be within the range of 0.13–0.38 Å by secondary structure matching (supplemental Table S2) (42), demonstrating that the overall structures are almost identical. Based on these results, we concluded that NylC$_A$ adopts a doughnut-shaped quaternary structure in which four heterodimer molecules are mutually related by a perpendicular crystallographic and/or non-crystallographic two-fold axis (Fig. 1). Contacts at the A/B and C/D interfaces (3,121 Å^2) were observed to be more extensive than those at the B/C and A/D interfaces (1,451 Å^2).

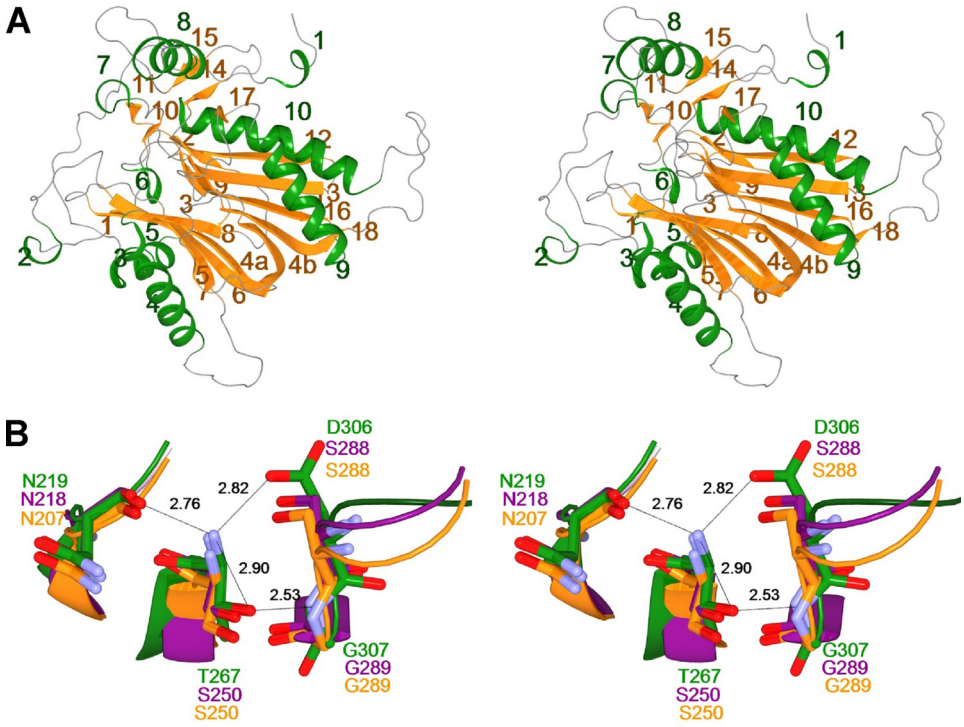

FIGURE 2. **Stereo view of subunit structure and catalytic center of NylC$_A$.** *A*, the overall structure of the heterodimer (molecule A) is shown as a *ribbon diagram*. Ten helices (H1–H10) and eighteen β-strands (S1–S18) are colored in *green* and *orange*, respectively. H1–H6 and H8–H10 are α-helices. H7 is a 3_{10} helix. *B*, the structure around the catalytic residue Thr-267 of NylC$_A$ (*green*) is superimposed onto the structure of DmpA (PDB ID code, 1B65; *magenta*) and BapA (PDB ID code, 3N33; *orange*). Possible hydrogen bonds in NylC$_A$ are indicated as *dotted lines* with the distances listed in angstroms.

Subunit Structure and Function Relationship with Other N-tn Family Enzymes

Each heterodimer contains 10 helices, H1–H10, which are α-helices with the exception of H7 (3_{10} helix), and 18 β-strands. The two subunits (α and β) obtained by intracleavage at Asn-266/Thr-267 are folded into a single domain, generating a stacked $\alpha\beta\beta\alpha$ core structure (Fig. 2*A*, supplemental Fig. S2). Namely, the central antiparallel β-sheet composed of five β-strands (β3, β4a, β5, β6, β7) and another antiparallel β-sheet composed of five β-strands (β4b, β12, β13, β16, β18) are packed against each other and connected by a common long β-strand (β4). These two sheets are flanked on one side by the α-helices H4 and H5 and on the other by α-helices H9 and H10. The $\alpha\beta\beta\alpha$ fold is typically conserved throughout the N-tn hydrolase superfamily (16–33). However, our data demonstrate that NylC differs from most N-tn hydrolases in the directionality and connectivity of its secondary structure elements.

To search for proteins that are evolutionary related to NylC, we performed a homology search based on the NylC$_A$ structure for PDB using the DALI program (43). The following four proteins (including one hypothetical protein) that exhibited high z-scores (z-score >14) were identified: L-aminopeptidase D-Ala-esterase/amidase from *Ochrobactrum anthropi* (DmpA; z-score = 26.3; PDB ID code: 1B65) (18), hypothetical D-aminopeptidase (z-score = 25.9; PDB ID code, 2DRH), β-peptidyl aminopeptidase from *Sphingosinicella xenopeptidilytica* (BapA; z-score = 25.2; PDB ID code: 3N33) (20), and ornithine acetyltransferase from *Streptomyces clavuligerus* (OAT; z-score = 14.1; PDB ID code: 1VZ6) (21) (supplemental Table S3). In contrast, the DALI z-scores of the other proteins in the PDB were determined to be below 8.

DmpA is an aminopeptidase that hydrolyzes peptides, with a preference for N-terminal residues in an L-configuration (L-Ala-Gly-Gly) and also amide or ester derivatives of D-Ala (19). BapA hydrolyzes β-oligopeptides and mixed β/α-oligopeptides with a β-amino acid residue at the N terminus (20). OAT is involved in the arginine biosynthetic pathway because it catalyzes the transfer of an acetyl group from *N*-acetylornithine to glutamate (21, 22). In contrast, NylC$_{p2}$ hydrolyzes Ahx cyclic and linear oligomers (degree of polymerization >3) but has no detectable activity with the 66 peptides tested (supplemental Table S4), including D,L-Ala-Gly-Gly (14, 15). Thus, NylC exhibits distinct substrate specificity from that of DmpA/BapA/OAT.

DmpA/OAT are considered to have a unique fold (designated as DOM-fold), which is different from that of most N-tn hydrolases (17). Based on fundamental topology differences, Cheng and Grishin (17) proposed that the functional similarities between DmpA/OAT and the other N-tn hydrolases result from convergent evolution rather than from having a common evolutionary origin. The fold of NylC is similar to that of DmpA/BapA, and the structurally superimposable regions comprise 259 residues (DmpA) and 264 residues (BapA) (supplemental Table S3). The r.m.s. deviations of the superimposed C_α atoms were calculated to be 2.0 Å (DmpA) and 2.0 Å (BapA) by secondary structure matching. However, the following major structural differences were found among the family enzymes.

In contrast to the single domain structure of NylC/DmpA/BapA, OAT is composed of two domains (supplemental Fig. S3).

NylC is superimposable with OAT domain 1 located at positions 1–258. OAT domain 2 is located at the C-terminal region and is composed of 124 residues that have a successive order of secondary structure (β10-H9-H10-H11-β11-β12-H12-β13-β14-H13). DmpA and BapA are longer than NylC at the C-terminal region of the β-subunit by 34 and 30 residues, respectively (supplemental Fig. S4).

Helix H8, which is located at the C-terminal region of the α-subunit, is unique in NylC. H8 and its linked loop region is flipped out to the surface of the adjacent molecules upon autoprocessing (Fig. 1*C*). In DmpA/OAT, the corresponding helix is absent. Furthermore, in BapA, the corresponding region (positions 236–245), which contains β14 and a loop, is folded within the same subunit molecule without flipping out to the adjacent molecule.

The N-terminal 26 residues, including H1, generate unique structure specifically found in NylC. Moreover, in OAT, N-terminal 48 residues, including H1-H2-β1-β2, are absent (supplemental Fig. S4).

A loop flanked by β-strand β18 and helix H10 in NylC (positions 317–333) spatially share different positions in Dmp (positions 299–318) and in BapA (positions 299–316). In OAT, the corresponding loop is absent, and β9 and H18 are combined with a single residue (Val-235) at the junction (supplemental Fig. S4).

In NylC, a long β-strand (β4a, β4b) constitutes a part of the central two β-sheets (Fig. 2*A*). However, in DmpA/BapA/OAT, the corresponding β-strand is divided into two β-strands (*e.g.* β2, β3 in DmpA), which are connected by a short loop and constitute each β-sheet (supplemental Fig. S4).

Residues Responsible for Autoprocessing and Catalytic Function

In DmpA, autoprocessing occurs between Gly-249 and Ser-250. Additionally, the newly generated N-terminal Ser-250 of the β-subunit plays the roles of both the nucleophile (hydroxyl group) and the general base (α-amino group) in catalytic reactions (18). In NylC, Thr-267 participates in a hydrogen-bonding network with Asn-219, Asp-306, and Gly-307 (backbone-N). The positions of these four residues are spatially similar to those of Ser-250, Asn-218, Ser-288, and Gly-289 (backbone-N) in DmpA, respectively (Fig. 2*B*). The catalytic nucleophile (Ser-250) and the surrounding residues (Asn-207, Ser-288, and Gly-289 (backbone-N)) are also conserved in BapA. These results indicate that Thr-267 is most likely responsible for the catalytic function of NylC. Assuming that auto-proteolysis of the NylC precursor proceeds in manner similar to that proposed for other N-tn hydrolases (23–27), the reaction would be initiated by nucleophilic attack of Thr-267-O_γ to Asn-266-C_α carbon, generating a tetrahedral intermediate. This intermediate would rearrange into an ester intermediate (N–O acyl shift) that is subsequently hydrolyzed by an adjacent water molecule, producing the active enzyme.

Structural Alterations Induced by Autoprocessing

The poor electron density distribution in the carboxyl-terminal region of the α-subunit (positions 261–267) of the active $NylC_A$ enzyme has prohibited the determination of a structural model. The C-terminal region of the α-subunit has not been identified by x-ray crystallographic analyses of DmpA/BapA/OAT (supplemental Fig. S4). In a three-dimensional model of $NylC_A$, the distance between Pro-260-C_α and Thr-267-C_α is estimated to be 32.6 Å (supplemental Fig. S2). The large distance suggests that the local structural alteration that occurs is accompanied by autoprocessing. Namely, the terminal region of the α-subunit, including helix H8 and Pro-260, at each subunit interface flips out toward the adjacent molecules (Fig. 1*C*). We speculate that the structural alteration is important for generating the catalytic center responsible for the hydrolysis of incoming substrates (6-aminohexanoate-oligomers). Structural alterations induced by autoprocessing have been reported for other N-tn hydrolases (25).

Effect of Amino Acid Substitutions on Protein Stability

Thermal denaturation experiments using CD showed that the T_m of $NylC_A$ and $NylC_K$ are 60 and 67 °C, respectively (Fig. 3, Table 2). These values are 8–15 °C higher than the T_m of $NylC_{p2}$ (52 °C). We have suggested that at least one among the five alterations (G111S, D122G, H130Y, L137A, V225M) in $NylC_A$ contributes to the increase in the thermostability of $NylC_{p2}$. Moreover, at least one of the 10 alterations (D36A, A41V, M50T, I60V, A62S, T230G, V231I, V257L, E263Q, G354A) in $NylC_K$ is estimated to contribute to the further increase in thermostability (supplemental Fig. S1) (5). The three-dimensional structure of $NylC_A$ shows that most amino acid residues that differ among the three NylC enzymes were found to be located at the interfaces between the subunits (Fig. 1*B*). To examine the effect of the amino acid substitutions on the thermostability of proteins, we individually replaced the residues in $NylC_{p2}$ with the corresponding $NylC_A$ or $NylC_K$ sequences.

A single amino acid mutation of either D122G or H130Y, which are located at the A/D interface, increased the T_m of $NylC_{p2}$ by 24 and 11 °C, respectively (Fig. 3, Table 2). However a single substitution of either G111S or L137A at the same interface decreases the stability by ~10 °C. Even more drastic effects were observed with the combinations of these mutations. D122G/H130Y double mutations in $NylC_{p2}$ enhanced the thermostability to 81 °C. Far-UV CD spectra showed very little change, even at 75 °C, for the $G^{122}Y^{130}$ mutant, whereas the parental $NylC_{p2}$ and $NylC_A$ enzymes denatured at 75 °C (supplemental Fig. S5). The addition of two further mutations, D36A/E263Q derived from $NylC_K$, to the $G^{122}Y^{130}$ mutant enhanced the T_m to 88 °C ($G^{122}Y^{130}A^{36}Q^{263}$ mutant; Fig. 3). Notably, we observed that more than 90% of the enzyme activity was retained even after incubation of the $G^{122}Y^{130}A^{36}Q^{263}$ mutant for 30 min at 70 °C. In contrast, an L137A mutation drastically decreased thermostability in the $G^{122}Y^{130}$ and $S^{111}G^{122}Y^{130}$ mutants by 27 °C. Similarly, a V225M single mutation decreased the protein stability and/or the expression level in cells because no protein was detected in the cell extracts that were prepared by expressing the M^{225}-mutant $NylC_{p2}$. However, the stabilization effect is altered by the combination of other amino acid alterations close to Met-225 because the V225M mutation, in the context of the $S^{111}G^{122}Y^{130}A^{137}$ quadruple mutant, recapitulates the sequence of $NylC_A$ and

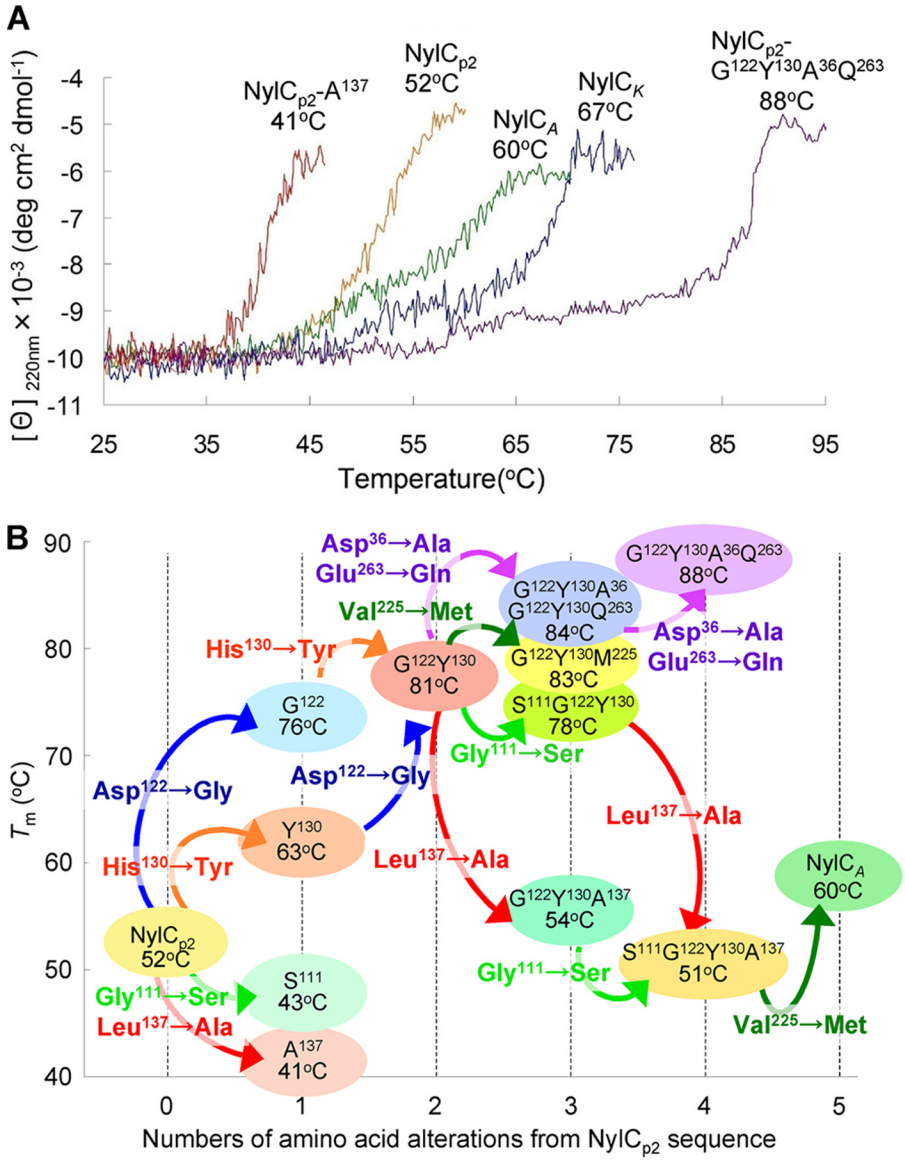

FIGURE 3. **Thermostability of NylC mutants.** *A*, thermal transition curves of the various NylC mutant enzymes. CD measurements were performed at 220 nm from 25 to 95 °C (1 °C min^{-1}). The results are expressed as the mean residue molar ellipticity [θ]. Protein concentrations of 0.1 mg ml^{-1} were used. *deg*, degree. *B*, the cumulative effects of amino acid mutations on the melting temperatures of denaturation (T_m) are shown.

improves its stability by 9 °C. Additionally, the V225M mutation in the G^{122}Y^{130} mutant improved the stability by 2 °C (see G^{122}Y^{130}M^{225}). These results demonstrate that subunit interactions that generate the quaternary structure drastically affect the thermostability of the enzyme (47 °C by five mutations; Fig. 3, Table 2).

Molecular Basis of Protein Stabilization

Based on the three-dimensional structure of NylC$_A$, we estimate that the following structural effects occurring at the subunit interfaces A/D (D122G, H130Y, L137A, G111S, and D36A) and A/B (V225M and E263Q) can cause changes in the thermostability of NylC$_{p2}$.

D122G—In NylC$_A$, Lys-159-NH$_3^+$ (in molecule A) is located 2.79 Å apart from Glu-115-COO$^-$ (in molecule D) (Fig. 4*A*). Therefore, the electrostatic effect between the two residues will enhance subunit binding around Gly-122 located on helix H4. However, in NylC$_{p2}$, the amino acid residue at position 122 is replaced with Asp, and the close proximity of the acidic residue Asp-122 (close to Glu-115) will reduce this stabilization effect.

H130Y and L137A—Tyr-130 (in molecule A) is located at a loop region (Arg-127–Ala-135) between helix H4 and β-strand β7 (supplemental Fig. S4). Tyr-130-O$_\eta$ forms a hydrogen bond with Glu-126-O$_\epsilon$ located at the end of helix H4 (Fig. 4*B*). Mutating Tyr-130 to His may destroy the hydrogen bonding and destabilize the loop. Therefore, a H130Y substitution in NylC$_{p2}$ will contribute to an increase in thermostability by stabilizing the loop region. In contrast, L137A substitution (in NylC$_{p2}$, G^{122}Y^{130} and S^{111}G^{122}Y^{130}) occurring at the same loop region resulted in the drastic decrease in the protein stability (Fig. 3*B*). Therefore, hydrophobic effect by Leu-137 should be involved in the stabilization of the loop region. Ala-137/Leu-137 affects the subunit interaction cooperatively with Gly-111/Ser-111 (Fig. 4*C*).

TABLE 2
Effect of amino acid substitutions on thermostability

Enzyme	Amino acid substitutions in $NylC_{p2}$ sequence	T_m
		℃
$NylC_{p2}$		52
$NylC_A$	G111S/D122G/H130Y/L137A/V225M	60
$NylC_K$	D36A/A41V/M50T/I60V/A62S G111S/D122G/H130Y/L137A/V225M T230G/V231I/V257L/E263Q/G354A	67
Single mutant		
$NylC_{p2}$-S^{111}	G111S	43
$NylC_{p2}$-G^{122}	D122G	76
$NylC_{p2}$-Y^{130}	H130Y	63
$NylC_{p2}$-A^{137}	L137A	41
$NylC_{p2}$-M^{225}	V225M	Not expressed
Double mutant		
$G^{122}Y^{130}$	D122G/H130Y	81
Triple mutant		
$G^{122}Y^{130}A^{36}$	D122G/H130Y/D36A	84
$G^{122}Y^{130}Q^{263}$	D122G/H130Y/E263Q	84
$G^{122}Y^{130}M^{225}$	D122G/H130Y/V225M	83
$S^{111}G^{122}Y^{130}$	G111S/D122G/H130Y	78
$G^{122}Y^{130}A^{137}$	D122G/H130Y/L137A	54
Quadruple mutant		
$G^{122}Y^{130}A^{36}Q^{263}$	D122G/H130Y/D36A/E263Q	88
$S^{111}G^{122}Y^{130}A^{137}$	G111S/D122G/H130Y/L137A	51

G111S—Hydrophilic Ser-111-O_γ (in molecule A) is surrounded by four hydrophobic residues (Tyr-98, Ala-137, Leu-139 (in molecule D) and Tyr-112 (in molecule A)) (Fig. 4*C*). Therefore, substitution from Ser-111 to Gly-111 (aliphatic small residue) should improve the hydrophobic stabilization effect at the A/D interface. In contrast, its reverse G111S substitution (in $NylC_{p2}$, $G^{122}Y^{130}$ and $G^{122}Y^{130}A^{137}$) actually reduces the thermostability (Fig. 3*B*).

D36A—Asp-36 (in molecule D) is located at helix H2, which is close to Glu-126 (in molecule A) (4.40 Å), whereas Asp-36 is replaced with Ala-36 in $NylC_K$ (Fig. 4*B*). Therefore, the D36A mutation will reduce electrostatic repulsion with Glu-126. Actually, D36A substitution (in $G^{122}Y^{130}$ and $G^{122}Y^{130}Q^{263}$) improves the thermostability (Fig. 3*B*).

V225M—Met-225 (in molecule A) does not directly contact with any adjacent subunits (Leu-9-$C_{\delta1}$ in molecule B is the nearest position; 5.29 Å). Met-225 is close to Gln-299 in the same subunit, which interacts with Arg-296-$N_{\eta2}$ (3.01 Å) (in molecule B) (Fig. 4*D*). Moreover, the position of Gln-299 should be stabilized by interaction with His-245-$N_{\epsilon2}$ (2.81 Å). Therefore, it is likely that amino acid substitution at position 225 indirectly affects the subunit interaction. Actually, V225M substitution (in $G^{122}Y^{130}$ and $S^{111}G^{122}Y^{130}A^{137}$) improves the thermostability (Fig. 3*B*), probably by generating a new interaction between Met-S_δ and Gln-299-$N_{\epsilon1}$ (3.56 Å) (Fig. 4*D*). However, it should be also noted that V225M substitution decreases the expression level and/or stability of $NylC_{p2}$ in the cell, as described above. Therefore, the total stabilization effects should be dependent on the combined interactions with the surrounding residues.

E263Q—Glu-263 is located at the terminal region of the α-subunit (Val-261–Asn-266), which had a poor electron density distribution in the x-ray diffraction study of $NylC_A$ (Fig. 1). In $NylC_K$, the acidic amino acid residue Glu-263 is replaced with neutral Gln, suggesting that altering the electrostatic environment induced by the E263Q mutation assists in improving subunit interactions.

Enzymatic Hydrolysis of Polymeric Nylon-6

Although the melting point of nylon-6 (220–225 °C) is much higher than the thermostability of the enzyme, performing the reaction at a high temperature should have the following advantages for the hydrolysis of nylon. 1) Hydrogen bonding between the polymer chains is partially weakened, allowing the enzyme to attack the polymer chains that are exposed to the solvent; and 2) the release of the cleaved fragments from the solid phase generates new sites for the subsequent reaction.

The mutated sites in the $G^{122}Y^{130}A^{36}Q^{263}$ quadruple mutant are located at the interface with other subunits and apart from catalytic Thr-267 (*e.g.* 26.6 Å to Gly-122 at C_α). Kinetic studies of the $G^{122}Y^{130}A^{36}Q^{263}$ mutant with the Ahx cyclic oligomer determined that the k_{cat} and K_m values are 2.8 ± 0.11 s^{-1} and 0.72 ± 0.06 mg ml^{-1}, respectively. When compared with the kinetic parameters of wild-type $NylC_{p2}$ (k_{cat} = 6.5 ± 0.29 s^{-1}; K_m = 3.7 ± 0.27 mg ml^{-1}) (5), these mutations decreased the turnover of the product but improved the affinity of the enzyme for the substrate. As a result, the calculated k_{cat}/K_m of the $G^{122}Y^{130}A^{36}Q^{263}$ mutant (3.9 s^{-1} ml mg^{-1}) is 2-fold higher than that of $NylC_{p2}$ (1.8 s^{-1} ml mg^{-1}). Based on the high thermostability and increasing catalytic activity of the $G^{122}Y^{130}A^{36}Q^{263}$ mutant, we considered this mutant to be suitable for testing the hydrolysis of polymeric nylon-6.

To increase the efficiency of nylon degradation, pellets of nylon-6 plastic were mechanically disintegrated to powder (diameter = 0.27 ± 0.14 mm, see "Experimental Procedures"). The powder was resuspended in buffer A (50 mg ml^{-1}), and the suspension was pretreated at 120 °C for 20 min. The enzyme reaction was performed using the $G^{122}Y^{130}A^{36}Q^{263}$ mutant (0.1 mg ml^{-1}) at 60 °C for 2 h.

SIMS measures the time of flight of the secondary ions generated by the bombardment of a sample with primary ion beams and sensitively detects the alterations in mass size occurring at the surface of solid particles (36, 44). We used gas cluster SIMS equipment, in which the primary ions are argon cluster

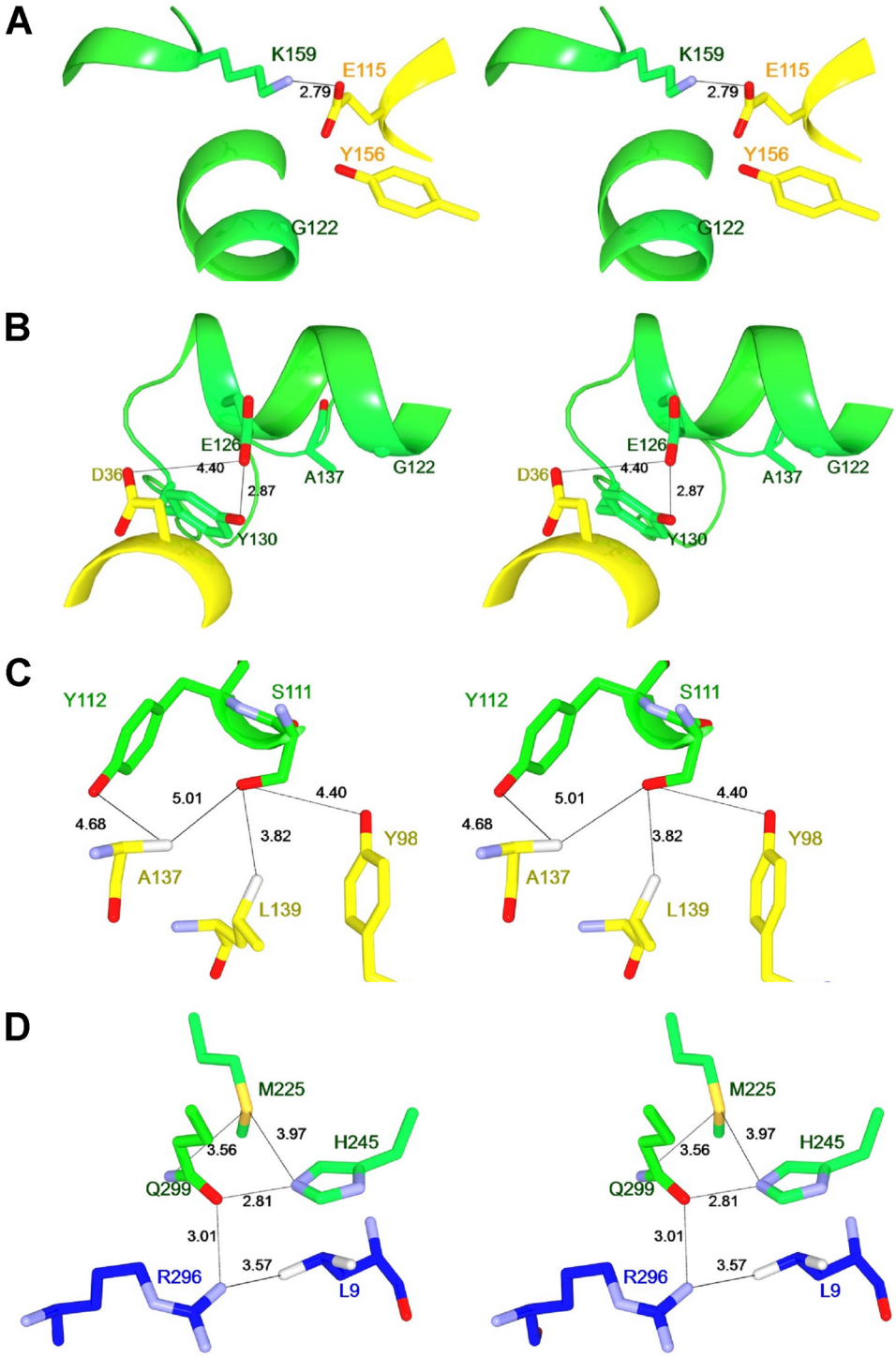

FIGURE 4. **Possible interactions at the subunit interfaces.** *A–D*, the possible interactions at the subunit interfaces around Gly-122 (*A*), Asp-36/Tyr-130 (*B*), Ser-111/Ala-137 (*C*), and Met-225 (*D*) are shown. Molecule A, molecule B, and molecule D in the quaternary structure are colored in *green*, *blue*, and *yellow*, respectively. Possible hydrogen bonds and contacts between two atoms are indicated as *dotted lines* with the distances listed in angstroms.

ions with a kinetic energy per atom controlled to be lower than 4 eV. This low energy of primary ions reduces the internal cleavage of polymer molecules, increasing the detection of the intact ions (36, 44). We observed a wide peak with an m/z range of 10,000–25,000 (top peak: 14,500) for untreated nylon-6, but the major peak was shifted to a smaller range with an m/z range of 8,000–23,000 (top peak: 13,000) for the reaction products (Fig. 5*A*). Moreover, SIMS analyses of the reaction products (dissolved in trifluoroethanol) revealed a new peak corresponding to an m/z range of 1,500–3,000 (top peak: 2,000; Fig. 5*B*). The presence of the specific fragments in the solid fraction demonstrated that NylC hydrolyzes nylon, but the fragments that were produced were still bound to polymer chains through hydrogen bonding (Fig. 6). These fragments corresponded to oligomers with 13–25 monomeric units, assuming an electric charge (z) = 1. In contrast, smaller fragments (<10 monomeric

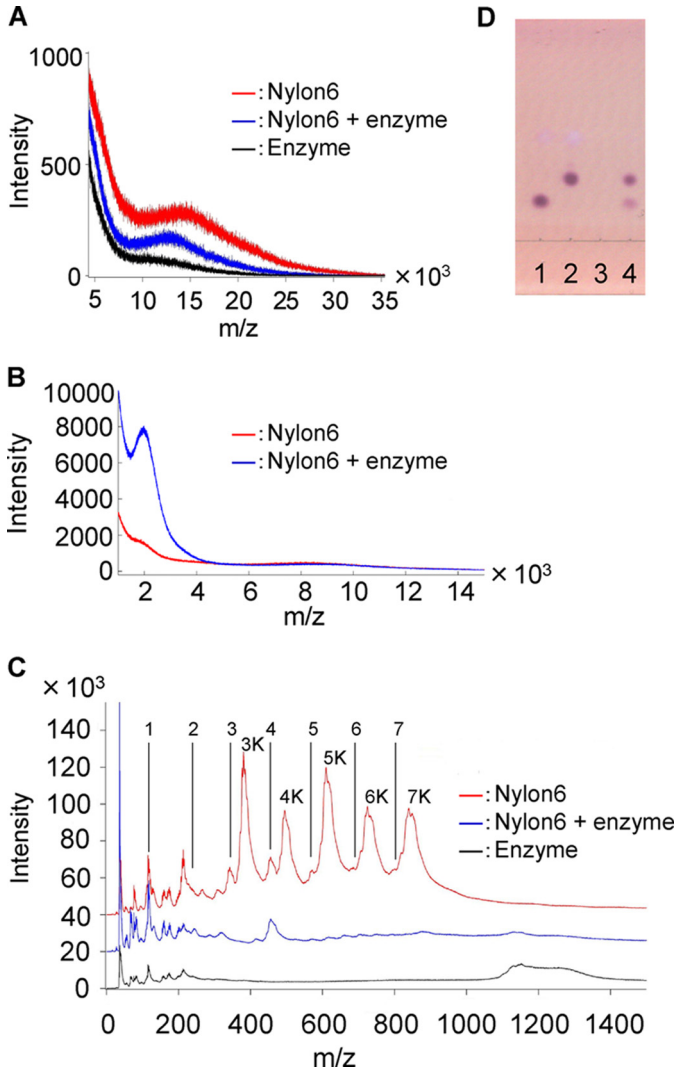

FIGURE 5. **Nylon degradation tests using argon cluster SIMS and TLC.** Nylon-6 powder (10 mg) was pretreated in triplicate in buffer A (180 μl) at 120 °C for 20 min. The $NylC_{p2}$-$G^{122}Y^{130}A^{36}Q^{263}$ mutant (1 mg ml^{-1}, 20 μl) was then added and incubated at 60 °C for 2 h. The experiment was performed in triplicate. *A*, the reaction products (both the soluble and the insoluble fractions) were spotted onto a silicon plate (1 cm^2). The *m/z* range of 5,000–35,000 was analyzed. *Red line*, pretreated nylon-6 at 120 °C in buffer A; *blue line*, enzyme-treated nylon-6; *black* line, enzyme alone. *B*, the solid fraction was washed with distilled water, lyophilized, and dissolved in trifluoroethanol (0.2 ml), and a fraction (0.02 ml) was spotted onto a silicon plate (1 cm^2). The *m/z* range of 1,500–15,000 was analyzed. *C*, the reaction products (both the soluble and the insoluble fractions) were spotted onto a silicon plate (1 cm^2). The *m/z* range of 0–1,500 was analyzed. The positions of Ahx monomer to heptamer (marked by *1–7*; *m/z* = 113, 226, 339, 452, 565, 678, 791) and those of the potassium-bound forms (marked by *3K–7K*) are shown. *D*, the soluble fractions (1 μl) were spotted onto a thin layer plate and developed, and the degradation products were detected by the ninhydrin reaction (5). *Slot 1*, 6-aminohexanoate; *slot 2*, 6-aminohexanoate-dimer; *slot 3*, pretreated nylon-6 at 120 °C in buffer A; and *slot 4*, enzyme-treated nylon-6.

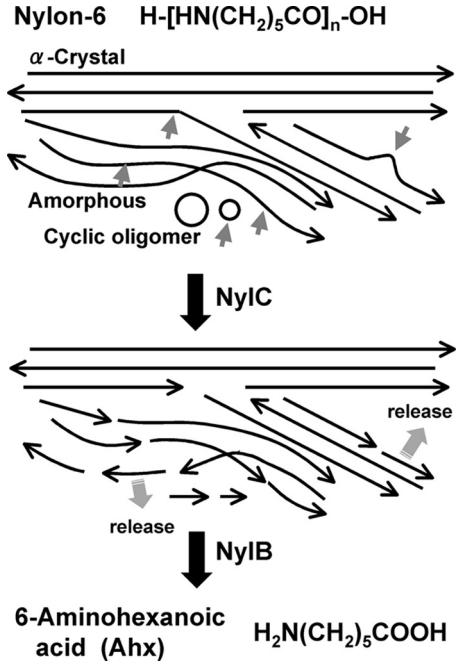

FIGURE 6. **Mode of nylon-6 degradation.** The polymer chains are stabilized by hydrogen bonds with adjacent chains aligned in the reverse orientation (*α-Crystal*) (1). Some chains constitute amorphous regions. The *circles* indicate the cyclic oligomers attached to the polymers. *Long arrows* indicate the direction of the polymer chains. *Short arrows* indicate cleavage by the enzyme. The 6-aminohexanoate-oligomers were converted to 6-aminohexanoate by the subsequent NylB reaction.

units) released from the solid fraction should be readily hydrolyzed to dimers and monomers (Fig. 5*C*). Consistent with this hypothesis, TLC analysis showed that the dimers and monomers are detected in the soluble fractions (Fig. 5*D*). Therefore, we confirmed that the dimers are converted to monomers by a subsequent NylB reaction.

The original nylon sample exhibited five major peaks (Fig. 5*C*, *3K–7K*), which are estimated to be potassium ion-bound forms, $[HN(CH_2)_5CO]_nK^+$ for Ahx trimer to heptamer (*m/z* = 378, 491, 604, 717, and 830), because the sample includes potassium ions in the reaction mixture and the cation-bound forms generally display a higher intensity than the unbound forms in the SIMS analysis (36). However, these peaks disappeared in the NylC-treated sample. Additionally, TLC analysis of the untreated nylon did not detect any spots by ninhydrin reaction. However, after NylC treatment, spots indicative of dimers and monomers were produced (Fig. 5*D*). From these results, we conclude that the Ahx cyclic oligomers were attached to the nylon sample and that these compounds were hydrolyzed by NylC (Fig. 6).

Potential Use in Industrial and Environmental Applications

Because SIMS analyses of the reaction products demonstrate that the thermostable NylC hydrolyzes polymeric nylon-6, we propose that NylC should be designated as nylon hydrolase (or nylonase) (EC 3.5.-.-). Notably, there is potential for the use of nylon hydrolysis in industrial and environmental applications, although the catalytic function and thermostability of NylC, as well as the pretreatment conditions of nylons for efficient hydrolysis, warrant further improvement.

Tools for Evaluation of Biodegradability of Polyamides

Ordinary biodegradability tests of polymers are performed in activated sludge (for 1 month) or in soil (for 4 months). Because the extent of hydrolysis of the polyamides by NylC is related to the biodegradability of the polyamide, an NylC reaction followed by SIMS analysis is appropriate for the prescreening of "biodegradable polyamides."

Improvement of Surface Structures of Nylon Fibers

Suitable methods to improve the surface structures of nylon remain poorly developed. With NylC, the partial enzymatic hydrolysis of nylon surfaces can be used to change the smoothness of nylon fibers.

Recycling of Nylons

Monomers (Ahx) obtained from nylon oligomers are aerobically metabolized in nylon oligomer-degrading strains (2–6). Suitable fermentation or biotransformation processes could enable the conversion of Ahx to other metabolites, such as organic acids or alcohols. Alternatively, Ahx may be a reusable reagent for the production of nylon-6 after conversion to ϵ-caprolactam by intramolecular dehydration. Therefore, the development of these processes could enable the recycling of nylons and decrease the environmental waste caused by the accumulation of man-made compounds.

Acknowledgment—Nylon-6 was a generous gift from Toyobo Co. Ltd. (Tsuruga, Japan).

REFERENCES

1. Dasgupta, S., Hammond, W. B., and Goddard, W. A., 3rd (1996) Crystal structures and properties of nylon polymers from theory. *J. Am. Chem. Soc.* **118,** 12291–12301
2. Negoro, S. (2000) Biodegradation of nylon oligomers. *Appl. Microbiol. Biotechnol.* **54,** 461–466
3. Okada, H., Negoro, S., Kimura, H., and Nakamura, S. (1983) Evolutionary adaptation of plasmid-encoded enzymes for degrading nylon oligomers. *Nature* **306,** 203–206
4. Kato, K., Ohtsuki, K., Koda, Y., Maekawa, T., Yomo, T., Negoro, S., and Urabe, I. (1995) A plasmid encoding enzymes for nylon oligomer degradation: nucleotide sequence and analysis of pOAD2. *Microbiology* **141,** 2585–2590
5. Yasuhira, K., Tanaka, Y., Shibata, H., Kawashima, Y., Ohara, A., Kato, D., Takeo, M., and Negoro, S. (2007) 6-Aminohexanoate oligomer hydrolases from the alkalophilic bacteria *Agromyces* sp. strain KY5R and *Kocuria* sp. strain KY2. *Appl. Environ. Microbiol.* **73,** 7099–7102
6. Yasuhira, K., Uedo, Y., Takeo, M., Kato, D., and Negoro, S. (2007) Genetic organization of nylon oligomer-degrading enzymes from alkalophilic bacterium, *Agromyces* sp. KY5R. *J. Biosci. Bioeng.* **104,** 521–524
7. Yasuhira, K., Shibata, N., Mongami, G., Uedo, Y., Atsumi, Y., Kawashima, Y., Hibino, A., Tanaka, Y., Lee, Y. H., Kato, D., Takeo, M., Higuchi, Y., and Negoro, S. (2010) X-ray crystallographic analysis of the 6-aminohexanoate cyclic dimer hydrolase: catalytic mechanism and evolution of an enzyme responsible for nylon-6 byproduct degradation. *J. Biol. Chem.* **285,** 1239–1248
8. Negoro, S., Ohki, T., Shibata, N., Mizuno, N., Wakitani, Y., Tsurukame, J., Matsumoto, K., Kawamoto, I., Takeo, M., and Higuchi, Y. (2005) X-ray crystallographic analysis of 6-aminohexanoate-dimer hydrolase: molecular basis for the birth of a nylon oligomer-degrading enzyme. *J. Biol. Chem.* **280,** 39644–39652
9. Ohki, T., Wakitani, Y., Takeo, M., Yasuhira, K., Shibata, N., Higuchi, Y., and Negoro, S. (2006) Mutational analysis of 6-aminohexanoate-dimer hydrolase: relationship between nylon oligomer hydrolytic and esterolytic activities. *FEBS Lett.* **580,** 5054–5058
10. Negoro, S., Ohki, T., Shibata, N., Sasa, K., Hayashi, H., Nakano, H., Yasuhira, K., Kato, D., Takeo, M., and Higuchi, Y. (2007) Nylon-oligomer-degrading enzyme/substrate complex: catalytic mechanism of 6-aminohexanoate-dimer hydrolase. *J. Mol. Biol.* **370,** 142–156
11. Kawashima, Y., Ohki, T., Shibata, N., Higuchi, Y., Wakitani, Y., Matsuura, Y., Nakata, Y., Takeo, M., Kato, D., and Negoro, S. (2009) Molecular design of a nylon-6 byproduct-degrading enzyme from a carboxylesterase with a β-lactamase fold. *FEBS J.* **276,** 2547–2556
12. Ohki, T., Shibata, N., Higuchi, Y., Kawashima, Y., Takeo, M., Kato, D., and Negoro, S. (2009) Two alternative modes for optimizing nylon-6 byproduct hydrolytic activity from a carboxylesterase with a β-lactamase fold: X-ray crystallographic analysis of directly evolved 6-aminohexanoate-dimer hydrolase. *Protein Sci.* **18,** 1662–1673
13. Negoro, S., Kakudo, S., Urabe, I., and Okada, H. (1992) A new nylon oligomer degradation gene (nylC) on plasmid pOAD2 from a *Flavobacterium* sp. *J. Bacteriol.* **174,** 7948–7953
14. Kakudo, S., Negoro, S., Urabe, I., and Okada, H. (1993) Nylon oligomer degradation gene, nylC, on plasmid pOAD2 from a *Flavobacterium* strain encodes endo-type 6-aminohexanoate oligomer hydrolase: purification and characterization of the nylC gene product. *Appl. Environ. Microbiol.* **59,** 3978–3980
15. Kakudo, S., Negoro, S., Urabe, I., and Okada, H. (1995) Characterization of endo-type 6-aminohexanoate-oligomer hydrolase from *Flavobacterium* sp. *J. Ferment. Bioeng.* **80,** 12–17
16. Oinonen, C., and Rouvinen, J. (2000) Structural comparison of Ntn-hydrolases. *Protein Sci.* **9,** 2329–2337
17. Cheng, H., and Grishin, N. V. (2005) DOM-fold: a structure with crossing loops found in DmpA, ornithine acetyltransferase, and molybdenum cofactor-binding domain. *Protein Sci.* **14,** 1902–1910
18. Bompard-Gilles, C., Villeret, V., Davies, G. J., Fanuel, L., Joris, B., Frère, J. M., and Van Beeumen, J. (2000) A new variant of the Ntn hydrolase fold revealed by the crystal structure of L-aminopeptidase D-Ala-esterase/amidase from *Ochrobactrum anthropi*. *Structure* **8,** 153–162
19. Fanuel, L., Goffin, C., Cheggour, A., Devreese, B., Van Driessche, G., Joris, B., Van Beeumen, J., and Frère, J. M. (1999) The DmpA aminopeptidase from *Ochrobactrum anthropi* LMG7991 is the prototype of a new terminal nucleophile hydrolase family. *Biochem. J.* **341,** 147–155
20. Geueke, B., Heck, T., Limbach, M., Nesatyy, V., Seebach, D., and Kohler, H. P. (2006) Bacterial β-peptidyl aminopeptidases with unique substrate specificities for β-oligopeptides and mixed β,α-oligopeptides. *FEBS J.* **273,** 5261–5272
21. Elkins, J. M., Kershaw, N. J., and Schofield, C. J. (2005) X-ray crystal structure of ornithine acetyltransferase from the clavulanic acid biosynthesis gene cluster. *Biochem. J.* **385,** 565–573
22. Sankaranarayanan, R., Cherney, M. M., Garen, C., Garen, G., Niu, C., Yuan, M., and James, M. N. (2010) The molecular structure of ornithine acetyltransferase from *Mycobacterium tuberculosis* bound to ornithine, a competitive inhibitor. *J. Mol. Biol.* **397,** 979–990
23. Okada, T., Suzuki, H., Wada, K., Kumagai, H., and Fukuyama, K. (2006) Crystal structures of γ-glutamyltranspeptidase from *Escherichia coli*, a key enzyme in glutathione metabolism, and its reaction intermediate. *Proc. Natl. Acad. Sci. U.S.A.* **103,** 6471–6476
24. Marc, F., Weigel, P., Legrain, C., Glansdorff, N., and Sakanyan, V. (2001) An invariant threonine is involved in self-catalyzed cleavage of the precursor protein for ornithine acetyltransferase. *J. Biol. Chem.* **276,** 25404–25410
25. Okada, T., Suzuki, H., Wada, K., Kumagai, H., and Fukuyama, K. (2007) Crystal structure of the γ-glutamyltranspeptidase precursor protein from *Escherichia coli*: structural changes upon autocatalytic processing and implications for the maturation mechanism. *J. Biol. Chem.* **282,** 2433–2439
26. Tikkanen, R., Riikonen, A., Oinonen, C., Rouvinen, R., and Peltonen, L. (1996) Functional analyses of active site residues of human lysosomal aspartylglucosaminidase: implications for catalytic mechanism and autocatalytic activation. *EMBO J.* **15,** 2954–2960
27. Guan, C., Liu, Y., Shao, Y., Cui, T., Liao, W., Ewel, A., Whitaker, R., and Paulus, H. (1998) Characterization and functional analysis of the cis-autoproteolysis active center of glycosylasparaginase. *J. Biol. Chem.* **273,** 9695–9702
28. Schmidtke, G., Kraft, R., Kostka, S., Henklein, P., Frömmel, C., Löwe, J., Huber, R., Kloetzel, P. M., and Schmidt, M. (1996) Analysis of mammalian 20 S proteasome biogenesis: the maturation of β-subunits is an ordered two-step mechanism involving autocatalysis. *EMBO J.* **15,** 6887–6898
29. Guo, H. C., Xu, Q., Buckley, D., and Guan, C. (1998) Crystal structures of *Flavobacterium* glycosylasparaginase: an N-terminal nucleophile hydrolase activated by intramolecular proteolysis. *J. Biol. Chem.* **273,**

20205–20212
30. Saarela, J., Oinonen, C., Jalanko, A., Rouvinen, J., and Peltonen, L. (2004) Autoproteolytic activation of human aspartylglucosaminidase. *Biochem. J.* **378,** 363–371
31. Michalska, K., Brzezinski, K., and Jaskolski, M. (2005) Crystal structure of isoaspartyl aminopeptidase in complex with L-aspartate. *J. Biol. Chem.* **280,** 28484–28491
32. Kim, Y., Yoon, K., Khang, Y., Turley, S., and Hol, W. G. (2000) The 2.0 Å crystal structure of cephalosporin acylase. *Structure* **8,** 1059–1068
33. Michalska, K., Hernandez-Santoyo, A., and Jaskolski, M. (2008) The mechanism of autocatalytic activation of plant-type L-asparaginases. *J. Biol. Chem.* **283,** 13388–13397
34. Yasuhira, K., Shibata, N., Tanaka, Y., Kumagai, N., Tanaka, Y., Nagai, K., Kato, D., Takeo, M., Negoro, S., and Higuchi, Y. (2011) Crystallization and X-ray diffraction analysis of nylon-oligomer hydrolase (NylC) from *Agromyces* sp. KY5R. *Acta Crystallogr. Sect. F Struct. Biol. Cryst. Commun.* **67**, 892–895
35. Sambrook, J., and Russell, D. W. (2001) *Molecular Cloning: A Laboratory Manual*, 3rd Ed., Cold Spring Harbor Laboratory Press, Cold Spring Harbor, NY
36. Mochiji, K., Hashinokuchi, M., Moritani, K., and Toyoda, N. (2009) Matrix-free detection of intact ions from proteins in argon cluster secondary ion mass spectrometry. *Rapid Commun Mass Spectrom.* **23,** 648–652
37. Otwinowski, Z., and Minor, W. (1997) Processing of X-ray diffraction data collected in oscillation mode. *Methods Enzymol.* **276,** 307–326
38. Weeks, C. M., Blessing, R. H., Miller, R., Mungee, R., Potter, S. A., Rappleye, J., Smith, G. D., Xu, H., and Furey, W. (2002) Towards automated protein structure determination: BnP, the SnB-PHASES interface. *Z. Kristallogr.* **217,** 686–693
39. de La Fortelle, E., and Bricogne, G. (1997) Maximum-likelihood heavy atom parameter refinement for multiple isomorphous replacement and multiwavelength anomalous diffraction methods *Methods Enzymol.* **276,** 472–494
40. McRee, D. E. (1993). *Practical Protein Crystallography*, Academic Press, San Diego, CA
41. Brünger, A. T., Adams, P. D., Clore, G. M., DeLano, W. L., Gros, P., Grosse-Kunstleve, R. W., Jiang, J. S., Kuszewski, J., Nilges, M., Pannu, N. S., Read, R. J., Rice, L. M., Simonson, T., and Warren, G. L. (1998) Crystallography & NMR system: a new software suite for macromolecular structure determination. *Acta Crystallogr. D Biol. Crystallogr.* **54,** 905–921
42. Krissinel, E., and Henrick, K. (2004) Secondary-structure matching (SSM), a new tool for fast protein structure alignment in three dimensions. *Acta Crystallogr. D Biol. Crystallogr.* **60,** 2256–2268
43. Holm, L., and Sander, C. (1993) Protein structure comparison by alignment of distance matrices. *J. Mol. Biol.* **233,** 123–138
44. Moritani, K., Mukai, G., Hashinokuchi, M., and Mochiji, K. (2009) Site-specific fragmentation of polystyrene molecule using size-selected argon gas cluster ion beam. *Appl. Phys. Express.* **2,** 046001

Three-dimensional Structure of Nylon Hydrolase and Mechanism of Nylon-6 Hydrolysis

Seiji Negoro, Naoki Shibata, Yusuke Tanaka, Kengo Yasuhira, Hiroshi Shibata, Haruka Hashimoto, Young-Ho Lee, Shohei Oshima, Ryuji Santa, Shohei Oshima, Kozo Mochiji, Yuji Goto, Takahisa Ikegami, Keisuke Nagai, Dai-ichiro Kato, Masahiro Takeo and Yoshiki Higuchi

J. Biol. Chem. 2012, 287:5079-5090.
doi: 10.1074/jbc.M111.321992 originally published online December 19, 2011

The three-dimensional structure of nylon hydrolase and its mechanism of nylon-6 hydrolysis

SUPPLEMENTARY DATA ONLINE

Legend for supplementary figures

Fig. S1. Comparison of amino acid sequences of NylC from *Arthrobacter* plasmid pOAD2 ($NylC_{p2}$), *Agromyces* ($NylC_A$) and *Kocuria* ($NylC_K$). Amino acid residues are shown as *one-letter* codes. Fifteen residues differed between $NylC_{p2}$ and $NylC_K$, of which the five residues in *green* boxes are altered in both $NylC_K$ and $NylC_A$. Ten residues in *blue* boxes are unique to $NylC_K$.

Fig. S2. Stereoview of the $NylC_A$ heterodimer shown as a ribbon diagram. The α-subunit and β-subunit in molecule A are colored in *dark green* and *light green*, respectively. The distance (32.6 Å) between Pro260 and Thr267 at C_α is shown.

Fig. S3. Stereoviews of overall structure of $NylC_A$. Superimposition of the $NylC_A$ structure (*green*) with L-aminopeptidase D-Ala-esterase/amidase from *Ochrobactrum anthropi* (DmpA: PDB ID code, 1B65; *magenta*) **(*A*),** β-peptidyl aminopeptidase from *Sphingosinicella xenopeptidilytica* (BapA: PDB ID code, 3N33; *orange*) (***B***), and ornithine acetyltransferase from *Streptomyces clavuligerus* (PDB ID code, 1VZ6; *yellow*) (***C***). Positions of N-terminus of α-subunit (α-N term), C-terminus of α-subunit (α-C term), N-terminus of β-subunit (β-N term) and C-terminus of β-subunit (β-C term) in $NylC_A$ are shown.

Fig. S4. Multiple three-dimensional alignment of $NylC_A$ and typical N-tn hydrolases. A multiple three-dimensional alignment was performed using secondary structure matching (SSM) of the following proteins (42): DmpA, L-aminopeptidase D-Ala-esterase/amidase (PDB ID code, 1B65); BapA, β-peptidyl aminopeptidase (PDB ID code, 3N33); and OAT, ornithine acetyltransferase (PDB ID code, 1VZ6). The secondary structures are shown as *green* (helix) or *orange* (β-strand) letters. The numbering of DmpA, BapA and OAT is the same as the numbering registered in the protein data bank. Helices and β-strands of $NylC_A$ shown in Fig. 2*A* are illustrated at the top with *green* cylinders (helix) and *orange* arrows (β-strand). The catalytic residue (nucleophile) is in yellow. Amino acid residues affecting the thermostability of $NylC_A$ (Asp36, Ser111, Gly122, Tyr130, Ala137 and Met225) are marked with asterisks. Because the residues of the regions of 261-266 of $NylC_A$ were not able to fit in the electron density map due to poor electron density distribution, they were excluded from the three-dimensional alignment.

Fig. S5. CD spectra at far UV (200-250 nm). *A*. CD measurements were carried out using a J-720WI spectropolarimeter (Jasco, Japan) at 25 °C. ***B***. A temperature shift from 25°C to 75°C (at 1°C min^{-1}) was performed. CD measurements were conducted at 75°C. A cuvette with a path length of 1 mm was used for all far UV CD measurements. The results are expressed as the mean residue molar ellipticity, [θ], and defined as $[\theta] = 100\ (\theta_{obs}-\theta_{back})\ l^{-1}\ c^{-1}$, where θ_{obs} is the observed ellipticity in degrees, θ_{back} is the observed ellipticity in degrees in the absence of enzyme (background), c is the molar concentration of the residue, and l is the length of the light path (in centimeters). The protein concentration used in all far UV CD measurements was 0.1 mg ml^{-1}.

Table S1. Sequences of primers used for the construction of NylC mutants.

Mutation	Oligonucleotide	5’ Sequence 3’
G111S	FEG111S	GGAGCC**AGC**TACGGGCTCGAGGCGGGC
	REG111S	CCCGTA**GCT**GGCTCCGCCGGCCAGGCA
D122G	FED122G	GGGGTGAGC**GGC**GCGCTCCTGGAACGCCTC
	RED122G	TTCCAGGAGCGC**GCC**GCTCACCCCGGCGCC
H130Y	FEH130Y	CTCGAG**TAT**CGCACCGGCTTCGCCGAGCTC
	REH130Y	GGTGCG**ATA**CTCGAGGCGTTCCAGGAGCGC
L137A	FEL137A	GCCGAG**GCC**CAGCTGGTGTCGTCGGCG
	REL137A	CAGCTG**GGC**CTCGGCGAAGCCGGTGCG
V225M	FV225M	GTGATC**ATG**GACCGCGCGGGCACGGTGGTG
	RV225M	GCGGTC**CAT**GATCACACCGACCGGGTTCGG
D36A	FD36A	GGCAAC**TCC**ACGATCAGCGCGATCGTC
	RD36A	GATCGT**GGA**GTTGCCGGCCTCGGTGACGGG
E263Q	FE263Q	GGCAAC**TGC**ACGATCAGCGCGATCGTC
	RE263Q	GATCGT**GCA**GTTGCCGGCCTCGGTGACGGG

Underlined bases indicate the mutated sites.

Table S2. The root mean square deviation of backbone structure among subunit molecules of NylC_A.

	A	B	C	D	E	F	G	H	I	J	K	L	M	N	O
A		0.3	0.29	0.24	0.26	0.22	0.2	0.27	0.23	0.29	0.14	0.24	0.19	0.27	0.15
B	0.3		0.37	.3	0.31	0.28	0.25	0.31	0.34	0.38	0.33	0.29	0.34	0.37	0.32
C	0.29	0.37		0.2	0.19	0.18	0.38	0.22	0.31	0.29	0.26	0.23	0.21	0.23	0.28
D	0.24	0.3	0.2		0.15	0.19	0.33	0.15	0.26	0.27	0.24	0.17	0.19	0.2	0.22
E	0.26	0.31	0.19	0.15		0.18	0.34	0.2	0.27	0.3	0.2	0.21	0.23	0.24	0.25
F	0.22	0.28	0.18	0.19	0.18		0.28	0.23	0.27	0.29	0.24	0.22	0.21	0.24	0.24
G	0.2	0.25	0.38	0.33	0.34	0.28		0.33	0.27	0.37	0.24	0.31	0.3	0.35	0.25
H	0.27	0.31	0.22	0.15	0.2	0.23	0.33		0.27	0.26	0.25	0.17	0.23	0.25	0.24
I	0.23	0.3	0.31	0.26	0.27	0.27	0.27	0.27		0.36	0.24	0.26	0.26	0.3	0.26
J	0.29	0.38	0.29	0.27	0.3	0.29	0.37	0.26	0.36		0.27	0.2	0.26	0.28	0.27
K	0.14	0.33	0.26	0.24	0.26	0.24	0.24	0.25	0.24	0.27		0.23	0.18	0.26	0.17
L	0.24	0.29	0.23	0.17	0.21	0.22	0.31	0.17	0.2	0.2	0.23		0.21	0.22	0.23
M	0.19	0.34	0.21	0.19	0.23	0.21	0.3	0.23	0.26	0.26	0.18	0.21		0.13	0.17
N	0.27	0.37	0.23	0.2	0.24	0.24	0.35	0.25	0.3	0.28	0.26	0.22	0.13		0.24
O	0.15	0.32	0.28	0.22	0.25	0.24	0.25	0.24	0.26	0.27	0.17	0.23	0.17	0.24	

The root mean square deviations (rmsd) (Å) between the fifteen molecules (A - O) at C_α were calculated by secondary structure matching (SSM).

Table S3. Search for proteins with analogous folds using the program DALI

PDB ID	Z	RMSD	LALI	NRES	%ID	PDB description
1B65	26.3	2.8	259	363	20	D-Aminopeptidase
2DRH	25.9	2.7	256	354	21	Hypothetical D-aminopeptidase (361aa long)
3N5I	25.4	3.1	264	371	19	β-Peptidyl aminopeptidase
3N33	25.2	3.6	267	367	18	β-Peptidyl aminopeptidase
3N2W	25.2	3.6	266	367	18	β-Peptidyl aminopeptidase
1VZ8	14.3	3.4	204	376	14	Ornithine acetyl-transferase
1VZ6	14.3	3.4	204	376	14	Ornithine aetyl-transferase
1VZ7	14.1	3.4	204	376	14	Ornithine acetyl-transferase
3IT4	7.3	2.7	136	193	9	Arginine biosynthesis bifunctional protein ArgJ

Z, Z-score (strength of structural similarity in S.D. above expected); RMSD, positional root mean square deviation of superimposed C_α atoms in angstroms; LALI, total number of equivalenced residues; NRES, Number of amino acids in the protein; %ID, percentage of sequence identity.

Table S4. Peptides used for analysis of substrate specificity of $NylC_{p2}$.

Dipeptide	Gly-Gly	Gly-L-Ala	Gly-L-Leu
	Gly-L-Phe	Gly-L-Pro	Gly-L-Val
	L-Ala-L-Ala	D,L-Ala-Gly	D,L-Ala-D,L-Asn
	L-Ala-L-Asp	L-Ala-L-His	D,L-Ala-D,L-Leu
	L-Ala-L-Val	L-Ala-L-Ile	L-Ala-L-Phe
	L-Ala-L-Pro	L-Ala-L-Thr	L-Ala-L-Trp
	L-Ala-L-Tyr	L-Ala-L-Glu	L-Ala-L-Lys
	L-Ala-L-Met	L-Ser-Gly	L-Ser-L-Ala
	L-Val-Gly	L-Val-L-Ala	L-Leu-L-Ala
	L-Leu-Gly	L-Leu-L-Tyr	L-Leu-L-Leu
	L-Pro-Gly	L-Pro-L-Ala	L-Phe-Gly
	L-Phe-L-Ala	L-Trp-L-Ala	L-Trp-Gly
	L-Tyr-Gly	L-Tyr-L-Ala	L-Asp-Gly
	L-Glu-L-Ala	L-Glu-L-Val	L-Met-Gly
	L-Met-L-Ala	L-His-Gly	L-His-L-Ala
	L-His-L-Leu	L-Lys-Gly	
Tripeptide	Gly-Gly-Gly	Gly-Gly-L-Ala	
	Gly-Gly-L-His	Gly-Gly-L-Phe	
	Gly-L-Pro-L-Ala	Gly-L-Leu-L-Tyr	
	Gly-D,L-Leu-D,L-Ala	Gly-L-Ala-L-Ala	
	L-Ala-L-Ala-L-Ala	D,L-Ala-Gly-Gly	
	D,L-Ala-D,L-Leu-Gly	L-Leu-Gly-Gly	
	Gly-L-Phe-L-Ala	L-Glu-L-Val-L-Phe	
	L-Ser-L-Gln-Gly		
Tetrapeptide	Gly-Gly-Gly-Gly		
Pentapeptide	Gly-Gly-Gly-Gly-Gly		
	L-Ala-L-Ala-L-Ala-L-Ala-L-Ala		
Hexapeptide	Gly-Gly-Gly-Gly-Gly-Gly		

$NylC_{p2}$ has no detectable activity with the 66 peptides shown in this table (ref. 14, 15).

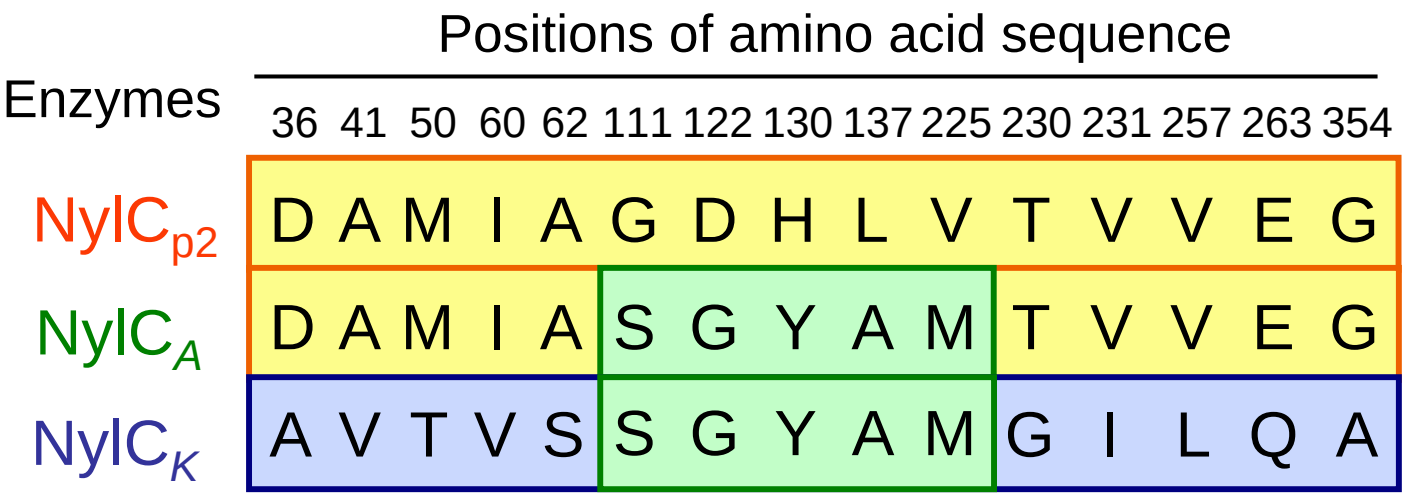
Positions of amino acid sequence
Enzymes
36 41 50 60 62 111 122 130 137 225 230 231 257 263 354
NylC$_{p2}$
D A M I A G D H L V T V V E G
NylC$_{A}$
D A M I A S G Y A M T V V E G
NylC$_{K}$
A V T V S S G Y A M G I L Q A

Fig. S1

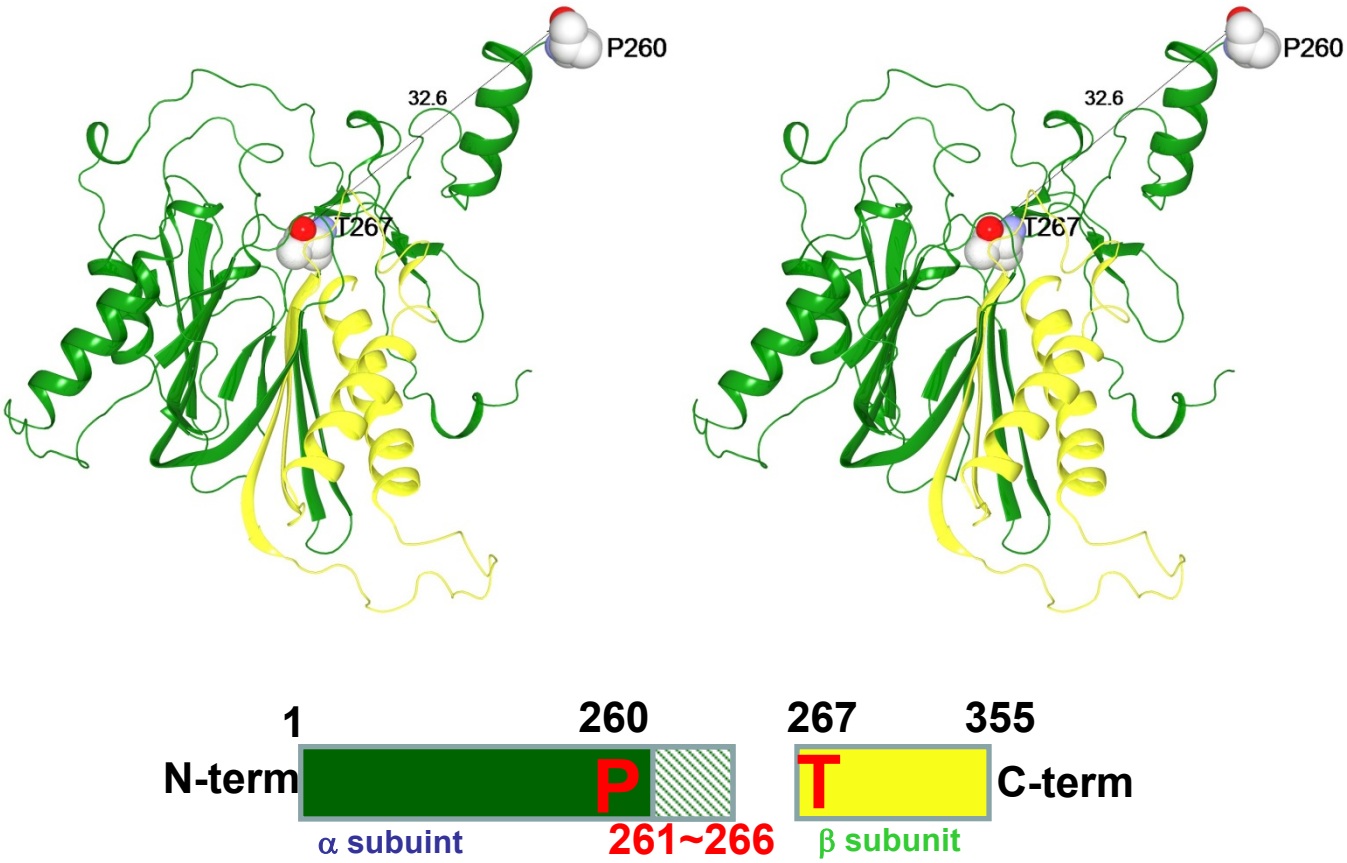
P260
32.6
T267
P260
32.6
T267
1
260
267
355
N-term
P
T
C-term
α subuint
261~266
β subunit

Fig. S2

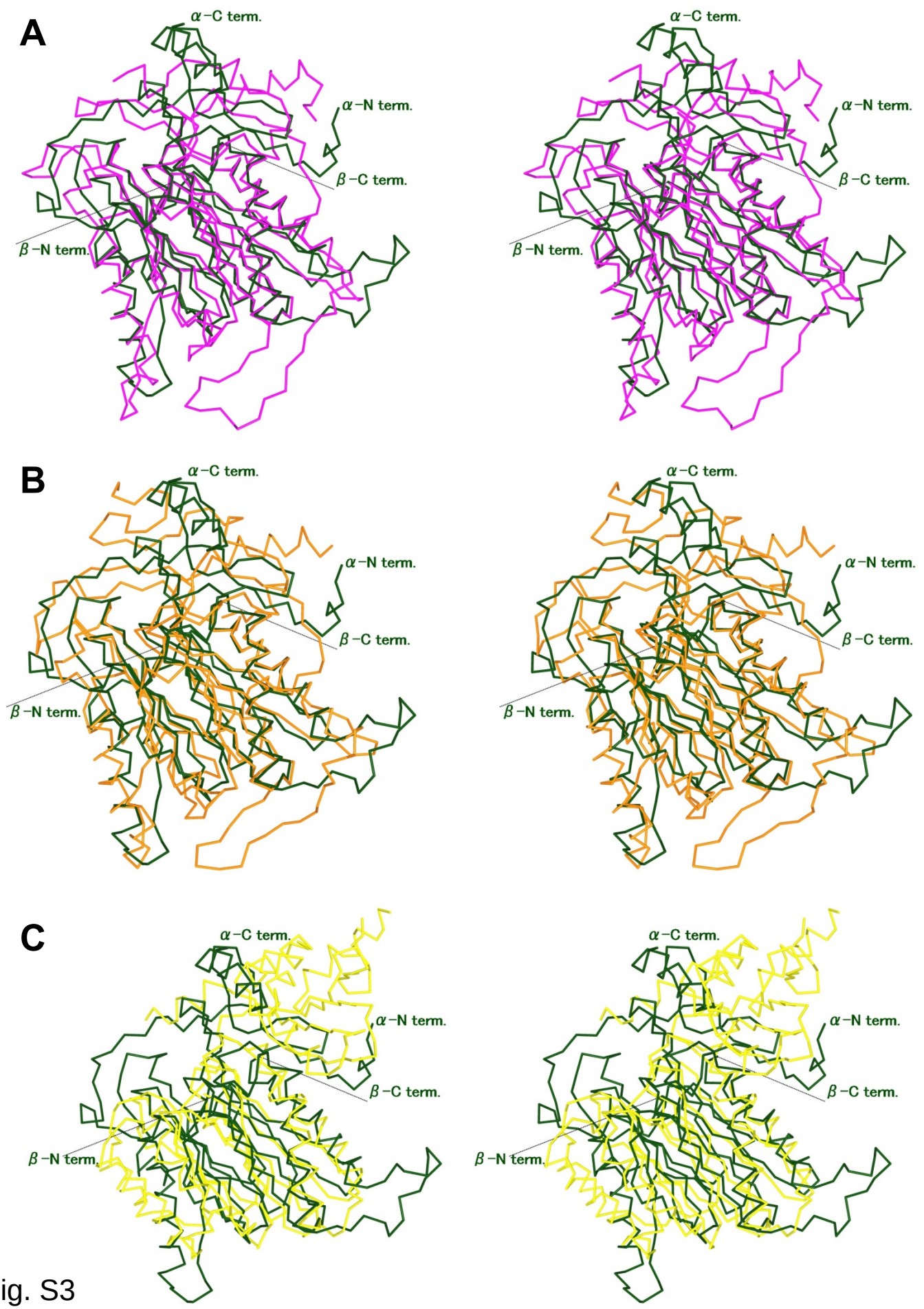
A
α –C term.
α –N term.
β –C term.
β –N term.
α –C term.
α –N term.
β –C term.
β –N term.
B
α –C term.
α –N term.
β –C term.
β –N term.
α –C term.
α –N term.
β –C term.
β –N term.
C
α –C term.
α –N term.
β –C term.
β –N term.
α –C term.
α –N term.
β –C term.
β –N term.

Fig. S3

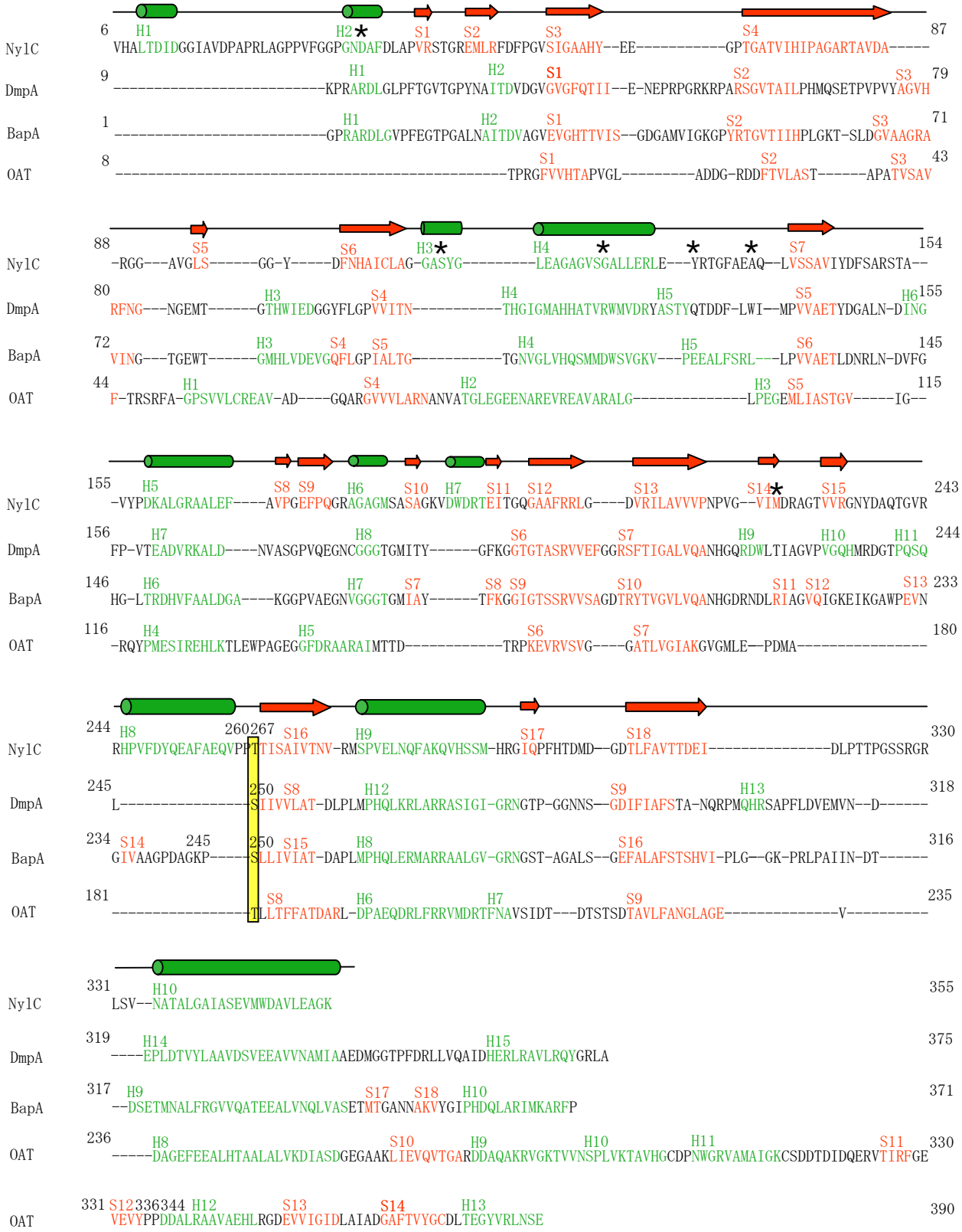

Fig. S4

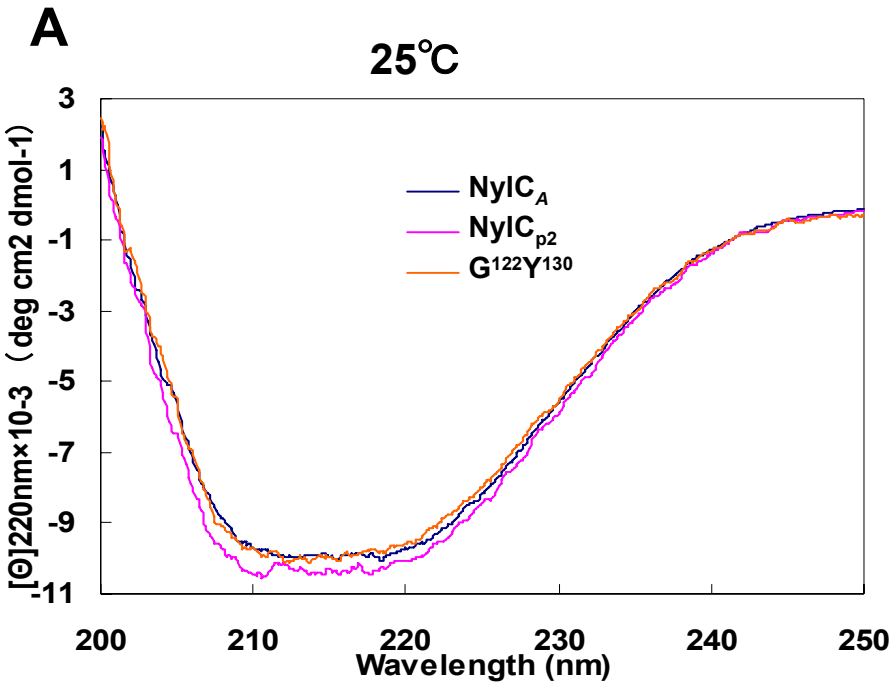
A
25℃
3
1
-1
-3
-5
-7
-9
-11
[Θ]220nm×10-3 （deg cm2 dmol-1）
NylC$_A$
NylC$_{p2}$
G^{122}Y^{130}
200
210
220
230
240
250
Wavelength (nm)

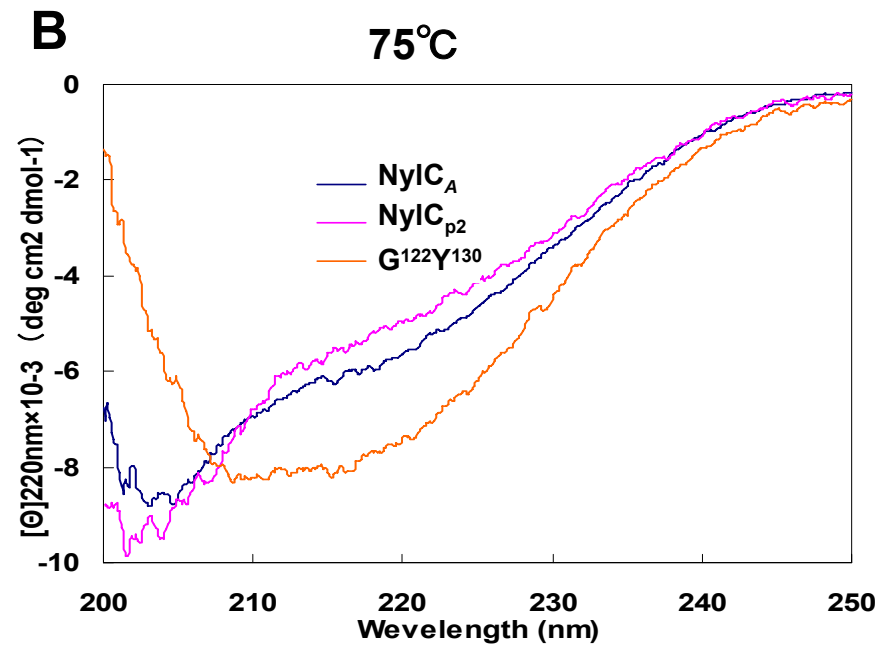
B
75℃
0
-2
-4
-6
-8
-10
[Θ]220nm×10-3 （deg cm2 dmol-1）
NylC$_A$
NylC$_{p2}$
G^{122}Y^{130}
200
210
220
230
240
250
Wevelength (nm)

Fig. S5